Applied Surface Science Advances 11 (2022) 100289

Contents lists available at ScienceDirect

Applied Surface Science Advances

journal homepage: www.sciencedirect.com/journal/applied-surface-science-advances

Recent advances on Z-scheme engineered $BiVO_4$-based semiconductor photocatalysts for CO_2 reduction: A review

Niqab Khan [a,b,#], Francielle Stelo [c,#], Gustavo H.C. Santos [d,b,#], Liane M. Rossi [d], Renato V. Gonçalves [b,*], Heberton Wender [c,*]

[a] Laboratory of Nanomaterials for Renewable Energy and Artificial Photosynthesis (NanoREAP), Programa de Pós-Graduação em Física (PPGFis), Federal University of Rio Grande do Sul (UFRGS), Campus do Vale, Agronomia, Porto Alegre-RS, Brazil
[b] São Carlos Institute of Physics, University of São Paulo, 13560-970 São Carlos, São Paulo, Brazil
[c] Nano&Photon research group. Laboratory of Nanomaterials and Applied Nanotechnology, Institute of Physics, Federal University of Mato Grosso do Sul, Av. Costa e Silva S/N, 79070-900, Campo Grande, MS, Brazil
[d] Departamento de Química Fundamental, Instituto de Química, Universidade de São Paulo, Av. Prof. Lineu Prestes 748, São Paulo 05508-000, SP, Brazil

A B S T R A C T

The designs of two or more absorber materials in a Z-scheme charge transfer configuration have paved the way for efficient CO_2 photoreduction to high-value chemicals and fuels using the artificial photosynthesis approach. Under visible light irradiation or natural solar illumination, semiconductors that themselves do not satisfy minimum thermodynamic requirements for CO_2 reduction or accompanying oxidation reactions can be used for targeted specific half-reactions. In this context, $BiVO_4$ has been extensively investigated for water oxidation showing promising activity under visible-light illumination but is restricted as a single reduction photocatalyst since its conduction band is not negative enough. This review provides an overview of the basic principles and fundamentals of CO_2 photoreduction and highlights the recent advances in the literature using $BiVO_4$-based Z-scheme photocatalysts. We show that using $BiVO_4$ as the oxidation photocatalyst, together with a reduction photocatalyst (Cu_2O, CdZnS, $ZnIn_2S_4$, $CuGaS_2$, g-C_3N_4, others) and under the Z-scheme charge transfer, is strategic for increasing visible-light absorption and facilitating charge separations while keeping the high redox potentials of the individual semiconductor components. This approach additionally helps to avoid undesired photocorrosion reactions triggered by trapped charges. Finally, some critical comments are raised for future research directions to improve CO_2 capture and photocatalytic conversion to green fuels and chemicals.

1. Introduction

A large portion of the energy (~80%) consumed in the world still comes from fossil fuels [1]. The dependency of energy production on the combustion of fossil fuels and the activities of human beings across the globe can result in emitting a high amount of carbon dioxide (CO_2) into the environment. The rapid emission of CO_2 into the environment leads to serious environmental issues like the greenhouse effect [2,3]. Approximately ~37Gt of CO_2 is emitted yearly and will likely reach up to ~43Gt by 2035 [4]. Also, according to the Intergovernmental Panel on Climate Change (IPCC) prediction, the average CO_2 emission will rise to 590 ppm by the year 2100 [5,6]. Such levels of CO_2 emission may raise the average earth's temperature and affect the sea level.

Resolving the environmental and energy crisis issues at once by capturing and converting CO_2 into other environmentally friendly hydrocarbon fuels is a great topic of interest [5,7]. However, high input energy is required to convert CO_2 into other molecules because the dissociation energy of the C=O bond is ~ 750 kJ mol^{-1}, which is much higher than other chemical bonds like C-C (~ 336 kJ mol^{-1}) and C-H (~ 430 kJ mol^{-1}) [8,9]. There are different approaches currently under development to accomplish the challenging CO_2 conversion, including thermochemical [10], electrochemical [11], photochemical [6,12–14], and hybrid systems [5,15,16]. Among them, the processes using solar energy are extremely appealing since it is one of the richest energy sources on the earth; around 1.3×10^5 TW of solar energy strikes the earth's surface, which is 10,000 times more than the current energy consumption [1]. Therefore, solar-driven CO_2 reduction, also known as artificial photosynthesis, is an alternative sustainable approach to overcome environmental issues and energy crises while converting CO_2 to high-value-added chemicals and fuels such as methanol, ethanol, methane, and formic acid [4,17]. However, the efficiency of artificial photosynthesis is very low and must be improved. The commercially available photovoltaic cells reached a solar energy conversion efficiency greater than 20%, so it has been suggested that solar-to-fuel efficiency of

* Corresponding authors.
E-mail addresses: rgoncalves@ifsc.usp.br (R.V. Gonçalves), heberton.wender@ufms.br (H. Wender).
# These authors contributed equally to this work.

https://doi.org/10.1016/j.apsadv.2022.100289
Received 9 March 2022; Received in revised form 8 August 2022; Accepted 9 August 2022
Available online 18 August 2022

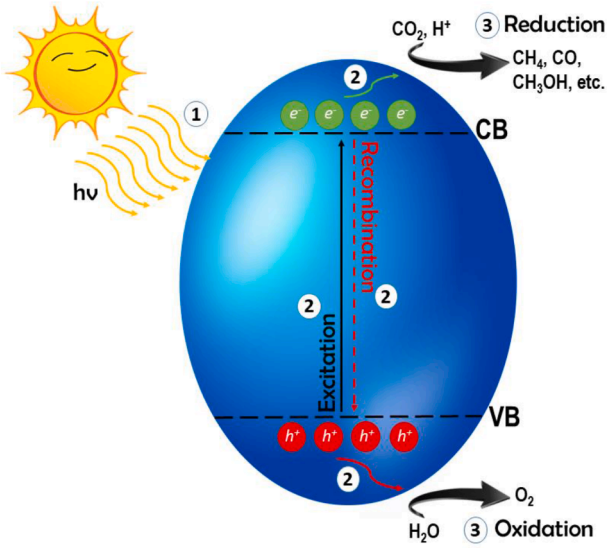

Fig. 1. Schematic illustrations of the three main steps (absorption, charge separation/migration/recombination, and redox reactions) involved in the reduction of CO_2.

Table 1
CO_2 reduction to different products and corresponding reduction potentials (V vs RHE).

Reactions	E (V vs RHE)	Equation
$CO_2 + 2H^+ + 2e^- \rightarrow HCOOH$	0.12	(1)
$CO_2 + 2H^+ + 2e^- \rightarrow CO + H_2O$	0.10	(2)
$CO_2 + 6\,H^+ + 6e^- \rightarrow CH_3OH + H_2O$	0.30	(3)
$CO_2 + 8H^+ + 8e^- \rightarrow CH_4 + 2H_2O$	0.17	(4)
$2CO_2 + 10H^+ + 10e^- \rightarrow CH_3CHO + 3H2O$	0.06	(5)
$2CO_2 + 12H^+ + 12e^- \rightarrow C_2H_5OH + 3H2O$	0.09	(6)
$2CO_2 + 12H^+ + 12e^- \rightarrow C_2H_4 + 4H2O$	0.08	(7)
$2CO_2 + 14H^+ + 14e^- \rightarrow C_2H_6 + 4H_2O$	0.14	(8)
$3CO_2 + 20H^+ + 20e^- \rightarrow C_3H_8 + 6H_2O$	0.09	(9)
$3CO_2 + 18H^+ + 18e^- \rightarrow C_3H_7OH + 5H_2O$	0.10	(10)

10% or above is the starting point for making artificial photosynthesis economically viable [18]. A deep discussion of the photocatalytic CO_2 reduction challenges can be accessed elsewhere [5,12,13,19,20].

Although many types of solar-active photocatalysts have been reported to reduce CO_2, many of them present low energy conversion efficiency, instability, uncontrolled selectivity, or incapability to completely suppress the hydrogen evolution reaction (HER) in the presence of water [21,22]. Therefore, it is highly challenging to design and fabricate highly active photocatalytic systems with high selectivity and efficiency for the CO_2 reduction reaction. The photocatalysis englobes three main steps in general: solar light harvesting, charge separation and transport, and surface reactions. Tremendous effort has been made to improve solar harvesting and charges separation and transportation steps for solar water splitting and CO_2 reduction [22–25]. Among the mainly investigated strategies to improve CO_2 photoreduction efficiency and selectivity, one can highlight the heterostructured dual absorber configuration [20,26,27], doping [28–30], defects engineering [31–33], and cocatalyst deposition [34–36]. Among these, heterojunctions are of particular interest because it not only improves solar light utilization but also facilitate charge separations and may maximize the redox ability from the combination of a reduction and an oxidation semiconductor photocatalyst, thereby improving the solar-to-fuel conversion efficiency.

Bismuth-based photocatalyst is a special and interesting class of materials among the visible-light-driven semiconductors for photocatalytic CO_2 which has been recently reviewed [37]. Bismuth vanadate ($BiVO_4$) is among the most effective solar-driven photocatalyst materials reported to date [38]. $BiVO_4$ has many interesting properties such as low bandgap, high chemical and physical stability, high absorption efficiency in the visible region, and low toxicity [39]. The low bandgap of $BiVO_4$ makes it capable of absorbing a large portion of visible light with a theoretical photocurrent density of 7.5 mA/cm^2 for water oxidation. Furthermore, assuming that all the photons with energies greater than 2.4 eV are absorbed, 9% of solar-to-hydrogen (STH) efficiency can be achieved [40]. Although $BiVO_4$ presents outstanding properties as an oxidation photocatalyst [41,42], its conduction band is not negative enough for conducting water or CO_2 reduction under solar light irradiation [37]. In addition, $BiVO_4$ applications for solar energy conversion are limited due to their low electron-hole separation efficiencies. Therefore, $BiVO_4$ heterostructured with a reduction photocatalyst under a Z-scheme is an interesting approach, since it will combine sunlight absorption abilities of both semiconductors, besides facilitating charge separations and preserving their original high redox strengths[43] for several photocatalytic applications. Here, we suggest to the reader some previous work on the advantages of using the Z-scheme configuration for solar energy conversion and applications in power generation [44,45], CO_2 photoreduction [26,46], solar water splitting [47,48], and degradation of organic pollutants [42,49].

This review article will focus on recent advances in using Z-scheme engineered $BiVO_4$-based semiconductor photocatalysts for accelerating and facilitating the charge separation efficiency aiming at a more efficient CO_2 reduction reaction.

2. Basic principles of artificial photosynthesis and CO_2 photoreduction

Photocatalytic CO_2 reduction is an artificial and pollution-free technique that utilizes solar energy and water to convert CO_2 into chemicals and fuels [50]. The process of photocatalytic CO_2 reduction occurs on the surface of a semiconductor material, characterized by a valence band (VB), a conduction band (CB), and a bandgap (forbidden band) [51]. Photocatalytic CO_2 reductions may occur after three widely accepted steps, as shown in Fig. 1.

(i) *Light absorption*: In the initial step (step 1), photons with energy equal to or greater than the photocatalysts' bandgap energy (Eg) are absorbed to excite an electron from the VB to the CB, leaving a hole (vacancy) in the VB, thus creating electron-hole pairs (e^-/h^+).

(ii) *Recombination*: in this step (step 2) the e^-/h^+pairs can either recombine in the bulk or move to the surface of the semiconductor. In a PEC configuration, the h^+ and the e^- separately and respectively migrate to the anode's surface and the cathode's surface (through the external circuit). Unfortunately, there is always a competition between charge separation and migration to the photocatalyst surface with charge recombination. Charge recombination can occur in the bulk as well as at the surface of the photocatalyst. It can be overcome by improving the crystallinity, lowering the number of defects, and increasing the conductivity of semiconductors [52].

(iii) *Surface chemical reaction*: in this step (step 3) those charge carriers which did not recombine in the bulk or at the surface may take part in oxidation or reduction reactions with different compounds available. To make surface reaction possible a photocatalyst must have appropriate VB and CB positions and appropriate active sites for redox reaction at the surface of photocatalysts [52].

Therefore, the redox ability of the free charges must be higher than the standard potentials in such a way that photogenerated electrons reduce CO_2 into products and holes oxidize the water into oxygen [53].

Photocatalysis provides a platform at ambient temperature and ambient pressure for CO_2 reduction, but still, it has some drawbacks to

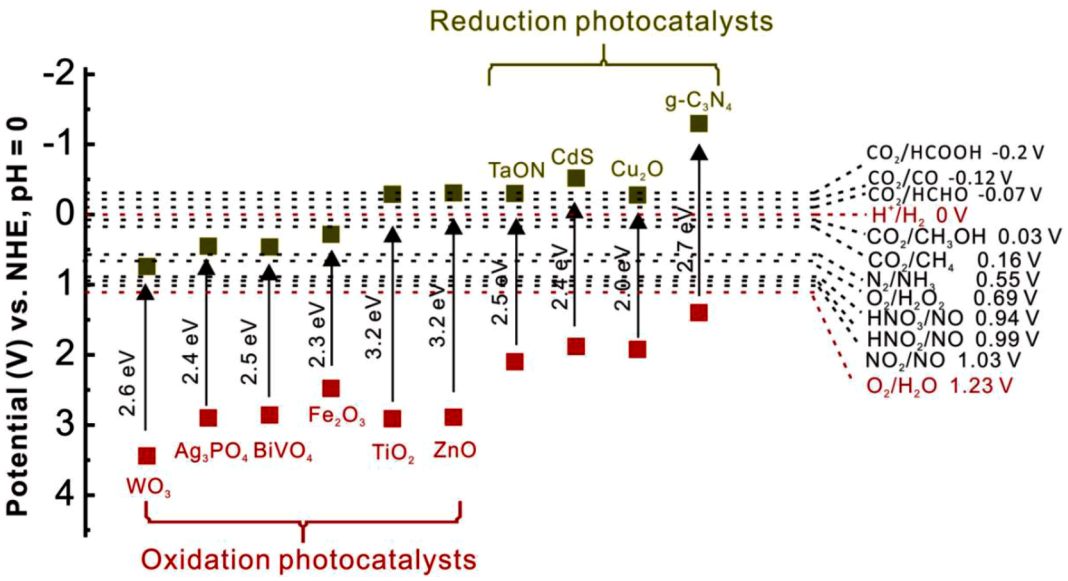

Fig. 2. Different bandgap energies of semiconductor photocatalysts for CO_2 reduction with redox potential vs. NHE at pH =0 [76].

overcome like poor light absorption, low yield, and photocorrosion of photocatalytic materials [15,54]. The poor light absorption problem is related to the fact that most materials with minimum thermodynamic conditions to reduce CO_2 and oxidize water present a wide bandgap and, therefore, need UV light to photogenerate charges [55]. Lower charge transfer, charge recombination, and inappropriate bandgap are the main contributors to the low photocatalytic CO_2 reduction yields [56,57]. Gibb's free energy of products must be lower than that of reactants for any chemical reaction, and it can be achieved while considering different parameters: light absorption, reactants concentrations, and applied electrochemical potential, among others. The reduction potentials *vs.* RHE for the conversion of CO_2 to other valuable products are given in Table 1 [12,13].

The reduction of CO_2 can result in many products, which depend on the reaction types and photocatalysts. As shown in Table 1, there are several reactions in which equations 1 to 4 represent C1 products and equations 5 to 10 represent C2+ products. The C1 products can be preferentially obtained when reduction of CO_2 occurs in a gaseous phase (mainly CH_4 or CO products). Due to the suppressed multiple electron transfer, CO_2 reduction selectivity is higher for C1 products in the majority of cases [13,14]. The recombination of e^-/h^+ is a general process that limits the multiple charge transfer in a short time and at a given location. The e^-/h^+ recombination can not only decrease the CO_2 reduction yield but also limits the selectivity of CO_2 towards CH_4 or CO. The materials that favor a large concentration of e^- photogeneration and storage can vary the selectivity towards C1 or C2 products; therefore, e^- and H^+ coupling lower than 8 leads to the C1 products and higher than 8 leads to C2+ products [58]. Till now, different materials have been used to increase the selectivity of CO_2 towards CH_4 and CO. Parul Verma et al. have used a metal-organic soft coordination polymer gel with nanoscroll morphology that exhibited higher selectivity of CO_2 towards CO (3.5 mmol $g^{-1}h^{-1}$) in the presence of TEA as a sacrificial electron donor. Similarly, they used 1-benzyl-1,4-dihydroni-cotinamide (BNAH) in combination with TEA as a sacrificial electron donor and improved selectivity (> 95%) of CO_2 towards CH_4 (6.7 mmol $g^{-1}h^{-1}$). Therefore, they demonstrated that covalent co-localization of photosensitizer and catalytic center is the main factor in CO_2 reduction [59]. SS Bhosali et al. have performed photocatalytic CO_2 reduction by bismuth-based perovskite nanocrystals at the gas-solid interface and obtained 14.9 μmol $g^{-1}$of CH_4 and 77.6 μmol g^{-1} of CO [60]. AA Beigi et al. have synthesized CdS/TiO_2 nanocomposites and investigated its photocatalytic CO_2 reduction selectivity towards CH_4 and O. The photocatalytic CO_2 reduction to CH_4 and CO was performed in a gaseous phase where the productivity of CO was five folds more than CH_4 [61]. RR Ikreedeegh et al. have synthesized RGO-linked g-C_3N_4/NH_2-MIL-125(Ti) nanocomposite that exhibited excellent CO_2 reduction to CH_4 and CO. The production of CO was 383.79 μmol g^{-1} in just 4 h irradiation time which was 5 times higher than of pure g-C_3N_4. The amount of CH_4 was also detected using the same reaction condition and found the total production of 13.8 μmol g^{-1} [62]. Besides C2+ products would be more valuable in the market than C1 products, the mechanism of CO_2 reduction to C2+ products is quite complicated, which involves many e^-/h^+ transfers and CO_2 activation reactions. The adsorption structure of CO_2 on catalyst surfaces is a key and determining primary step of CO_2 activation, and a series of steps take place after that, including charge transfer, formation of the intermediates, the cleavage of the C-O bond, and the formation of C-C and C-H bonds [63]. Shortly, materials that will result in a large number of photogenerated electrons would be more favorable materials to produce C2+ products [13].

The conversion of CO_2 into different products using solar energy as a driving force has drawn much attention since reported by Heilmann [8]. There are mainly two systems for CO_2 reduction. The first system (photochemical - PC) utilizes solar light and a particulate photocatalyst in the presence of a solvent to reduce the already dissolved CO_2, or in the gas phase, and convert it to other proper forms. This kind of system is a very convenient way for CO_2 reduction because it only depends on solar light as the driving force. However, oxidation and reduction occur on the same catalyst surface, and the recombination of the products from CO_2 with holes or produced oxygen may occur [64]. It can be avoided by using hole scavengers (H_2O_2, Na_2SO_3, alcohol, *etc.*) with their additional cost to the whole process. Another system for CO_2 reduction is the PEC, which mainly consists of three electrodes, a semiconducting electrode, also known as a working electrode, a counter electrode, and a reference electrode. In the PEC system, the half-cell reaction is performed by interacting light with the photoelectrode generating charge carriers to reduce CO_2, whereas the other half-cell oxidation reaction occurs at the counter electrode. Proton exchange membrane (in most cases Nafion) is helpful to separate oxidation and reduction products, which increases the efficiency of the PEC system. Similarly, the charge separation process can be improved by providing external bias, with the additional cost of electrode preparation and the input energy [53].

The main difference between CO_2 reduction and water splitting is the surface reaction of the photogenerated electrons. Proton reduction occurs in parallel with CO_2 reduction only in the presence of water [9].

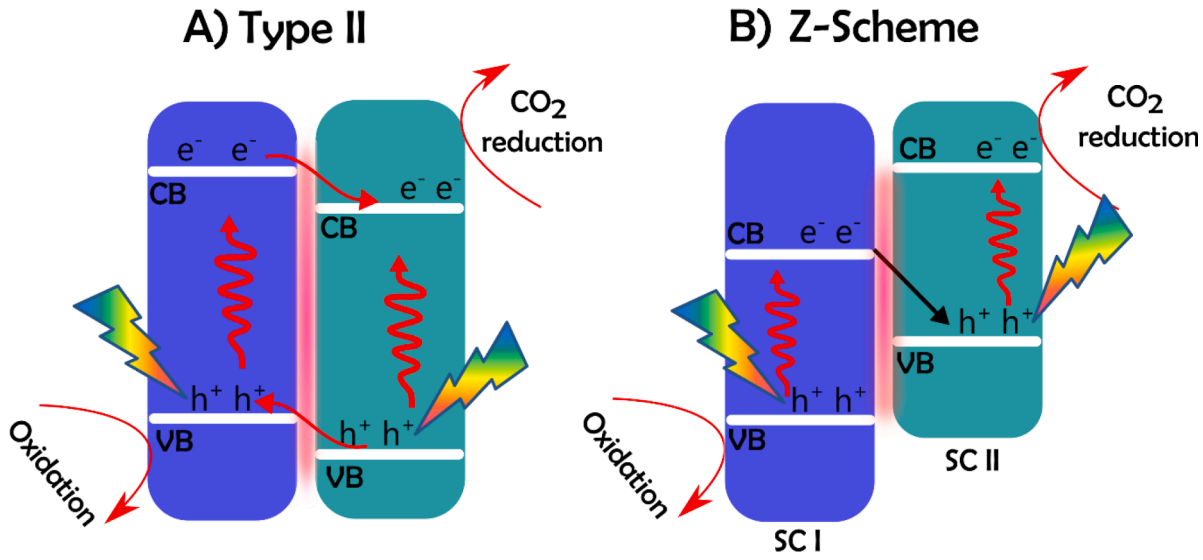

Fig. 3. a) Type-II heterojunction and b) Direct Z-scheme (or S-scheme) photocatalytic charge transfer mechanism for CO_2 reduction.

Two reaction arrangements are used to reduce CO_2, i.e., the liquid and gas phases. In the liquid phase, the carbon reduction is carried out mainly using the saturated aqueous solution of carbon dioxide. One of the crucial problems of the liquid phase is the limited solubility of CO_2 in the water, affecting the efficiency of CO_2 reduction [65]. The solubility of the CO_2 can be increased by the addition of carbonates and bicarbonates ($NaHCO_3$, or Na_2CO_3) in the aqueous solution. In the liquid phase, water reduction is difficult to avoid because of the preferable surface adsorption of water over CO_2. In the gaseous phase, the reaction is carried out in a CO_2-based atmosphere with some added amount of water that vaporizes in dry conditions [1]. Xie et al. [66] used TiO_2 and Pt-TiO_2 as photocatalysts to reduce CO_2 in gaseous and liquid phase arrangements. The efficiency of CO_2 reduction to CH_4 and hydrogen was tested. It was found that the production of CH_4 is three times higher in the gaseous phase setup than in the liquid, whereas hydrogen production is lower in the former.

2.1. *Semiconductor photocatalysts*

Many semiconductor photocatalysts have been developed to transform CO_2 into fuels and chemicals by the photoreduction process. The unique electronic properties of semiconductors are strongly related to their VB and CB energies. These band positions and structures are critical in semiconductors because they determine light absorption and redox reactions [64,67]. Solar light (photons) having energy equal to or greater than the E_g of the semiconductor can induce the creation of electron-hole pairs that further migrate to the material surface. These electron-hole pairs can be captured in the way – by the defects in the material both on the surface or the bulk –, recombine each other, or be converted to heat delivering new photons of lower energies. If these undesirable reactions can be partially overcome, those photogenerated charges may drive the photocatalytic reaction on the surface of semiconductors [68]. The mechanism of the solar-driven CO_2 reduction and water splitting reactions are the same up to some extent. The main difference is the desirable and competing reduction reaction, CO_2 reductions *vs.* proton reduction. Therefore, much attention was given to adjusting the mentioned properties of materials to reduce CO_2.

In terms of the redox ability, the positioning of VB and CB will dictate if the material is a reduction or an oxidation photocatalyst, Fig. 2. If the CB is negative enough compared to the standard reduction potentials of CO_2/water, the semiconductor is called a reduction photocatalyst (Cu_2O, CdS, g-C_3N_4, TaON, etc.). The opposite occurs when the VB is positive enough compared to the standard potential of water oxidation, where the semiconductor is called an oxidation photocatalyst ($BiVO_4$, WO_3, Fe_2O_3, etc.). As presented in Fig. 2, TiO_2 is a reduction and oxidation photocatalyst at the same time, but it is only possible at the cost of losing visible light absorption. In other words, TiO_2 applicability is limited under natural or artificial solar light. In this scenario, many visible light-responsive semiconductor materials have recently been reported for CO_2 reductions, such as $BiVO_4$ [69,70], ZnTe [71,72], $InTaO_4$, Cu_2O [73], graphitic-C_3N_4 [74], and $CuFeO_2$ [75]. Besides, different strategies have in parallel been established to increase the efficiency of photocatalyst for CO_2 reduction, such as using cocatalyst, dopants, defects, and heterojunctions (dual-absorbing configuration, topic of later discussion) [1].

The efficiency of CO_2 photoreduction can be affected by the deposition of some metallic cocatalysts such as Pt, Ag, Au, Cu, and Pd. It is essential to mention that these metallic cocatalysts are helpful to further accelerate the photoreduction reaction by receiving electrons from the semiconductor photocatalysts. As CO can be a subproduct of CO_2 reduction, Ag NPs have an excellent activity towards CO_2 reduction because of their weak bond with CO; meanwhile, Pt is poisoned by CO [53]. In the previously reported work by Iizuka et al., Ag was loaded on $ALa_4Ti_4O_{15}$ (A = Ca, Sr, and Ba) for the CO_2 reduction in water [34], and the authors showed that O_2 evoluted in a stoichiometric ratio indicating that water was consumed as electron donor and CO was the main reduction product on the optimized Ag/$BaLa_4Ti_4O_{15}$ photocatalyst. Additionally, bimetallic cocatalyst has high efficiency towards CO_2 reduction in the presence of water and sunlight irradiation. The loading of Cu-Pt as a cocatalyst on the TiO_2 was an efficient strategy to reduce CO_2 to different products (CH_4, C_2H_4, C_2H_6, etc.) in the presence of water and solar light illumination [77]. More details on the use of cocatalysts for improving semiconductors' charge separation and CO_2 reduction selectivity and activity can be found in the literature [35,36].

Doping wide bandgap semiconductor photocatalysts with different elements to change their optical and electrical properties is another strategy to improve CO_2 photoreduction efficiency. For example, doping TiO_2 with N or Ce can cause a red-shift of light absorption, increasing the activity [53]. N-doped TiO_2 showed an increased CO_2 reduction activity towards CH_4 [78]. Similarly, doping $NaTaO_3$ with different metals (Ba, Ca, Mg and Sr) improves the CO_2 reduction into CO in the presence of Ag cocatalysts. It was found that Ba-doped $NaTaO_3$ showed superior activity among all the other studied dopants towards CO_2 reduction (nearly 90% selectivity) [79]. A detailed discussion of doping to semiconductor materials for CO_2 reduction can be found in some recent article reviews and is outside the scope of this text [28–30].

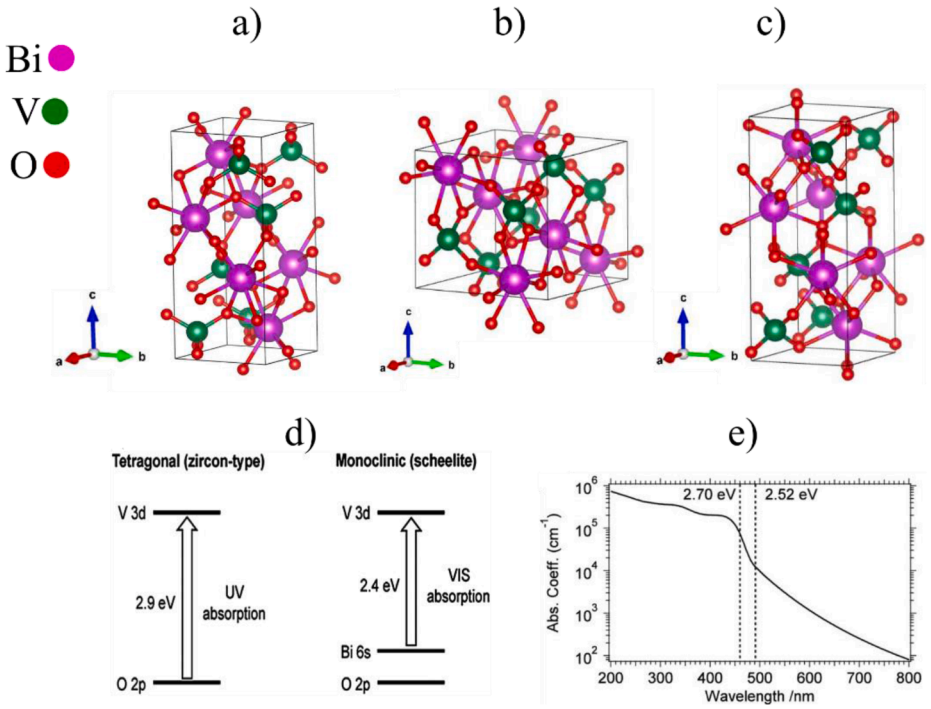

Fig. 4. Crystal structure of $BiVO_4$: (a) tetragonal scheelite, (b) tetragonal zircon, (c) monoclinic scheelite. Band structures of monoclinic scheelite and tetragonal zircon $BiVO_4$ (d) [93], and absorption coefficient of monoclinic $BiVO_4$ (e) [90].

In photocatalysis, defects are critical since they may change the photocatalysts' surface properties. Defects may change the interaction between the surface of the photocatalyst and the targeted molecule, consequently helping to lower the reaction activation energy. Density and type of defects have various impacts on photocatalytic activity. Oxygen vacancies on the surfaces of oxides and hydroxides are the most common defects which affect photocatalytic CO_2 reduction [31,32]. According to the literature, oxygen vacancies can absorb CO_2 molecules [80]. Different semiconductors with rich structural defects have been investigated for CO_2 photoreduction. Wang et al. used the defective CeO_2 for CO_2 photoreduction, resulting in ~4 μmol g^{-1} h^{-1} of CO. The authors proposed that the oxygen vacancies at the photocatalyst surface captured CO_2, lowering the reaction barrier [33]. Also, Ye et al. synthesized $SrTiO_3$ powder with Ti^{+3} ions and oxygen vacancies. They showed that these vacancies boosted the photocatalyst's visible light absorption and increased the chemical adsorption of CO_2 on both the surface and bulk phase of the photocatalyst [31].

2.2. Heterojunctions and the direct Z-scheme configuration

Heterostructures are the combination of two or more semiconductors and are a wide strategy to improve light absorption, redox ability, and charge separation in photochemical systems. It is worth mentioning that only a few single photocatalysts fulfill the minimum required thermodynamic criteria for an ideal photocatalyst, while most of them absorb only UV light.

Depending on the CB and VB energy positions of the individual semiconductors, heterostructures may be classified into three types: type I (straddling gap), type II (staggered gap), and type III (broken gap) [49,81]. Herein, we will focus the discussion on the type II case where charge separation is favorable for photocatalytic reactions. For more applications and fundamental definitions of these photocatalyst configurations, one can refer to a recent review article [49]. Briefly, type II heterostructures are among the most valuable because they boost charge separation by transferring electrons/holes from one material to another and, therefore, they are considered special charge separation heterostructures [82]. There are two possibilities for charge transfer in a type II heterostructure. In the first, electrons transfer from one material to another, coming from the more negative to the more positive CB, and holes do the opposite, i.e., move from the more positive to the more negative VB potential. This charge separation configures a common type-II heterojunction that can physically separate electrons and holes, which are represented in Fig. 3a. However, the common type-II heterojunction is not the most efficient strategy for charge separation since electrons move to a less reducing potential and holes migrate to a less oxidizing potential and, therefore, redox ability is decreased [49]. It is important to highlight that several works report improved photoactivity when engineering two or more semiconductor materials in a type II heterostructured charge separation mechanism. However, there will always be cases where the loss of redox ability limits the success of target reactions. Therefore, it is interesting and desirable to physically achieve charge separation by maintaining electrons and holes' highest possible redox potential, as observed in a special mechanism of charge transfer involving staggered gap semiconductors, known as direct Z-scheme.

The direct Z-scheme (or S-scheme) photocatalysts (Fig. 3b) have emerged as a promising strategy for CO_2 photoreduction. The S-scheme is a particular case of the more general Z-scheme when the semiconductors are directly connected to each other and charge separation is not mediated by other material. Due to their dual absorber engineering, Z-schemed photocatalysts combine sunlight absorption abilities and high charge separation while preserving the original high redox strengths [43]. Therefore, an artificial Z-scheme photocatalyst can overcome the challenges of charge recombination of single component photocatalysts and, at the same time, enhance optical properties and redox ability [83]. The Z-scheme system consists of at least two semiconductors, i.e., one dedicated to reduction reactions and the other to oxidation. Fig. 3b shows the oxidation semiconductor (SC I) with lower VB and the reduction semiconductor (SC II) with higher CB.

The basic principle of the Z-scheme involves the primary irradiation of two semiconductors, where electrons are excited from their VB to their CB after absorption of solar light photons with energy equal to or higher than their bandgaps. If photoexcited electrons in the CB of SC I recombine with holes in the VB of SC II, strong oxidative and reductive abilities in the photogenerated holes and electrons are respectively

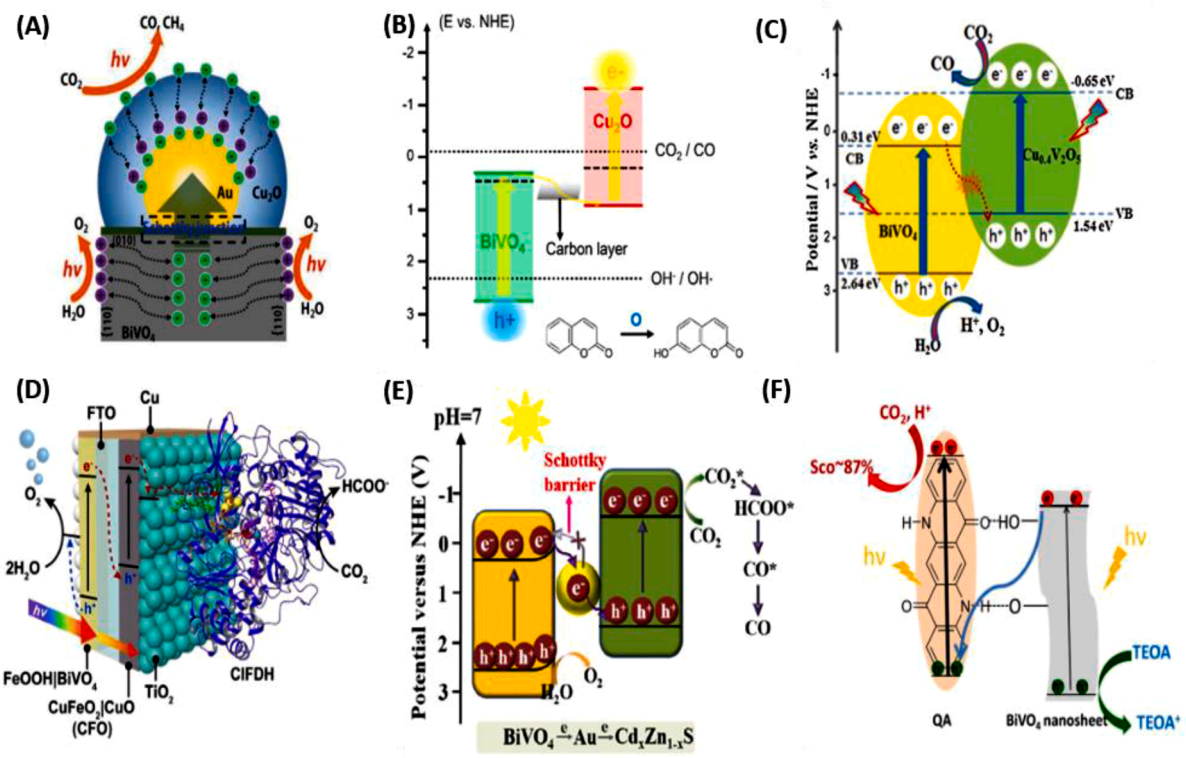

Fig. 5. Z/S-scheme proposed to describe the charge transfer mechanism of (A) $BiVO_4${010}-Au-Cu_2O; (B) BVO/C/Cu_2O; (C) $BiVO_4/Cu_{0.4}V_2O_5$; (D) FeOOH|$BiVO_4$|| ClFDH-TiO_2|CFO; (E) $Cd_{0.5}Zn_{0.5}S$@Au/$BiVO_4$; and (F) QA/10$BiVO_4$ [97,98,100–103].

preserved, as shown in Fig. 3b. The recombination of electrons from SC I with holes in SC II can be achieved in an all-solid-state configuration in two ways, i.e., by directly connecting both semiconductors (direct Z-scheme or S-scheme), or through a solid conductor (usually Au, Pt, Ag, etc.), known by solid mediator Z-scheme. It is also possible to perform charge transfer in solution using a redox couple, which was the first idea of the Z-scheme and is called redox-mediated Z-scheme [49].

The following sections will present a detailed discussion of using $BiVO_4$ under the Z/S-scheme configuration for photocatalytic CO_2 reduction.

3. $BiVO_4$ main properties

Naturally, $BiVO_4$ is found in an orthorhombic crystalline structure, known as pucherite, while synthetic $BiVO_4$ presents mainly three crystal structures: monoclinic scheelite (m-s), tetragonal scheelite (t-s), and tetragonal zircon (t-z), as shown in Fig. 4a-c [84]. Four and eight O atoms coordinate the V and Bi ions, respectively, in all three structures. Scheelite and zircon structures, however, differ by the Bi bounding to the VO_4 tetrahedra, i.e., Bi ions are surrounded by eight (or six) VO_4 tetrahedra in scheelite (or zircon) phases. Similarly, scheelite phases differ by the V-O bonds, where t-s structure consists of a V-O bond length of 1.72 Å, and m-s consists of two different V-O bond lengths of 1.77 Å and 1.69 A° [84]. Among these structures, the m-s $BiVO_4$ is preferred for photocatalysis and photoelectrocatalysis because of its thermodynamic stability and higher photoactivity under visible light illumination [41, 42]. The better photocatalytic response of the m-s $BiVO_4$ compared to t-z is due to the additional states formed by the Bi 6s and O 2p orbitals above the VB, lowering the bandgap from 2.9 (t-z) to 2.4 eV (m-s), as shown in Fig. 4d [85]. The DFT calculations also demonstrated that $BiVO_4$ is an indirect bandgap semiconductor where the top of the VB consists of Bi 6s and O $2p_\pi$ states and the estimated CB of V $3dx^2_y$ and dz^2 states [86]. The literature related to the optical transition of m-s $BiVO_4$ is controversial, with many experimental and computational data reporting both direct and indirect bandgap [86–88]. Recently, the indirect nature of the optical bandgap is a consensus as investigated by DFT and many spectroscopic techniques like X-ray Photoelectron Spectroscopy (XPS), Resonant Inelastic X-ray Spectroscopy (RIXS), X-ray Absorption Spectroscopy (XAS), Ultraviolet-visible (UV-vis) Spectroscopy, and ellipsometry [89,90]. Following different synthesis methods, experimental data has shown that m-s $BiVO_4$'s bandgap ranges from 2.4 to 2.5 eV [91]. The optical bandgap of catalytic semiconductors can be determined using a Kubelka–Munk estimation method after measuring the sample's reflectance [52]. The absorption coefficient of the m-s $BiVO_4$ increases from 1 $\times 10^4$ cm^{-1}at the band edge absorption onset of 500 nm to 1 $\times 10^5$ cm^{-1} at 460 nm (Fig. 4e). The yellow color of the $BiVO_4$ is related to the strong absorption of green to ultraviolet photons and transmission of yellow to infrared photons [91].

$BiVO_4$ is a photocatalyst used in many reactions, including the light-induced degradation of organic pollutants, water splitting, and CO_2 reduction. In photocatalytic water splitting, the photogenerated holes of $BiVO_4$ are used to oxidize water molecules to produce O_2. However, due to its low CB, $BiVO_4$ cannot reduce water or CO_2 molecules when applied as a single photocatalyst. Here comes the importance of the dual-absorber Z/S-scheme configuration, where $BiVO_4$ can act as the oxidation catalyst (e.g., for water oxidation) coupled to another semiconductor that will conduct CO_2 photoreduction reactions and convert CO_2 to other useful molecules, such as CO, methanol, ethanol, etc. [92].

4. $BiVO_4$-based Z-scheme photocatalysts for photocatalytic CO_2 reduction

This section presents the most recent and relevant research studies reported on $BiVO_4$-based Z-scheme photocatalysts for CO_2 photoreduction. Since the promising reported results of $BiVO_4$ photocatalysts for water oxidation half-reaction, the engineering of two or more semiconductor materials for increasing solar light hastening and improving charge separation and transfer while keeping high redox potentials of

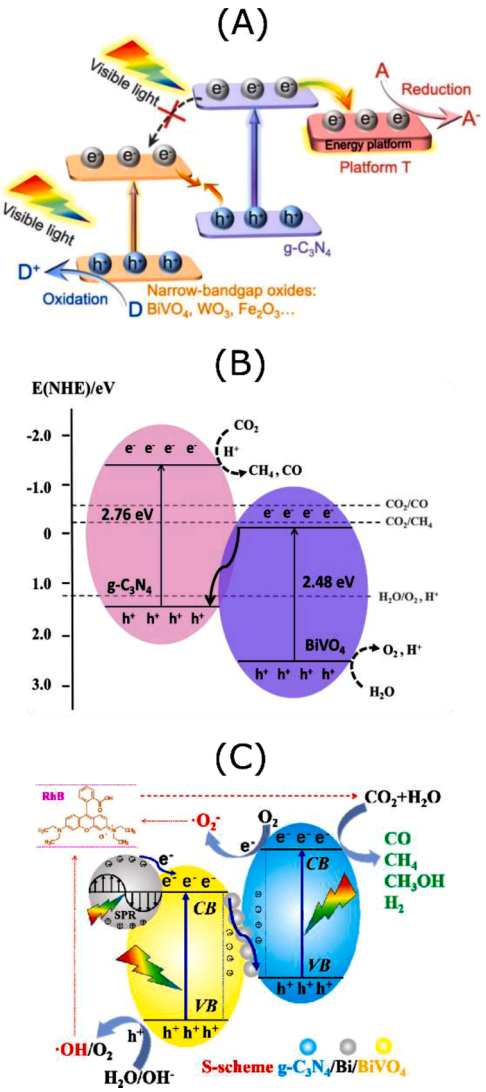

Fig. 6. A Z/S-scheme proposed to describe the charge transfer mechanism of (A) (001) TiO_2-g-C_3N_4/$BiVO_4$ (B) g-C_3N_4/$BiVO_4$ and (C) g-C_3N_4/Bi/$BiVO_4$ [104–106].

photoelectrons and holes is vital to enhancing CO_2 to fuel conversion under photocatalytic conditions.

An exciting material with suitable band energy positions for composing a Z-scheme charge transfer mechanism with $BiVO_4$ is Cu_2O. More than that, it is well-known that Cu_2O is a promising photocatalyst for CO_2 reduction under visible light illumination because of its favorable bandgap energy and its high negative conduction band [94–99]. In fact, a perfect match of energy band levels can be obtained between Cu_2O and $BiVO_4$, with the construction of a spontaneous path for charge separation. Zhou et al. recently reported a high-performance $BiVO_4${010}–Au–Cu_2O solid-mediated Z-scheme heterojunction that involves a facet-dependent Schottky-junction as an efficient electron-transfer route. In the preparation process of $BiVO_4${010}–Au–Cu_2O, first $BiVO_4$ truncated octahedron with different coexposed crystal facets, i.e. {010}, and {110}, were prepared via solid-state reaction, and then photoreduction method was employed to deposit Au or Cu_2O on the surface of already prepared $BiVO_4$ to obtain $BiVO_4${010}–Cu_2O or $BiVO_4${110}–Au. Finally, following the same procedure, $BiVO_4${010}–Au–Cu_2O was obtained. The truncated octahedron-shaped morphology was observed for $BiVO_4$ followed by a Cu_2O shell decorated with Au particles layer [98]. Compared to pristine materials, the heterostructure presented a superior activity for converting CO_2 to either CH_4 or CO, with rates of 3.15 or 2.08 μmol g^{-1} h^{-1}, respectively. It is worth noting that depositing Cu_2O–Au nanoparticles over the {010} planes of $BiVO_4$ provided a superior activity for CO_2 reduction. The authors claimed that the transfer of photoexcited electrons at the $BiVO_4$–Au interfaces to Cu_2O determines the charge-separation efficiency and controls the photoreduction activity of the Z-scheme system. For the $BiVO_4${010}–Au–Cu_2O, electron migration from $BiVO_4$ to Cu_2O resulted in more holes in Cu_2O that $BiVO_4$ electrons could consume. Thus, the photogenerated charge recombination and self-oxidation process ($Cu^+ + h^+ \rightarrow Cu^{2+}$) were simultaneously suppressed, producing enhanced stability and better photocatalytic activity. Fig. 5a shows the mechanism proposed by the authors for CO_2 and CH_4 evolution over the $BiVO_4${010}–Au–Cu_2O photocatalyst [98].

In another work, 3D Cu_2O nanowire arrays (NWAs) were explored to construct a Z-scheme with $BiVO_4$ particles [97]. Cu_2O NWAs were prepared by anodization, and carbon was deposited by immersion in a glucose solution followed by annealing. After that, the as-prepared C/Cu_2O NWAs were immersed in an aqueous solution of $BiVO_4$ (BVO) precursors to form the final solid-mediated Z-scheme BVO/C/Cu_2O NWAs. The CO_2 photoreduction tests were conducted in the gaseous phase with vaporized H_2O at 40°C, under irradiation of a 300 W Xe lamp with a cut-off filter (> 420 nm) [97]. BVO/C/Cu_2O NWAs produced mainly CO at a rate of ~3.01 μmol g^{-1} h^{-1}. This value is 4.7 and 9.4 times higher than those obtained with Cu_2O NWAs and Cu_2O mesh, respectively. The deposition of C enhanced the CO formation rate by a 1.4 factor and resulted in the simultaneous evolution of CH_4. In the absence of the $BiVO_4$, the C/Cu_2O NWAs performed 3.3 times worse than the complete Z-scheme system (Figure 5b). Interestingly, after five cycles, the Z-scheme heterojunction retained 98% of the activity observed for the first cycle, while a decrease to 60% was observed when

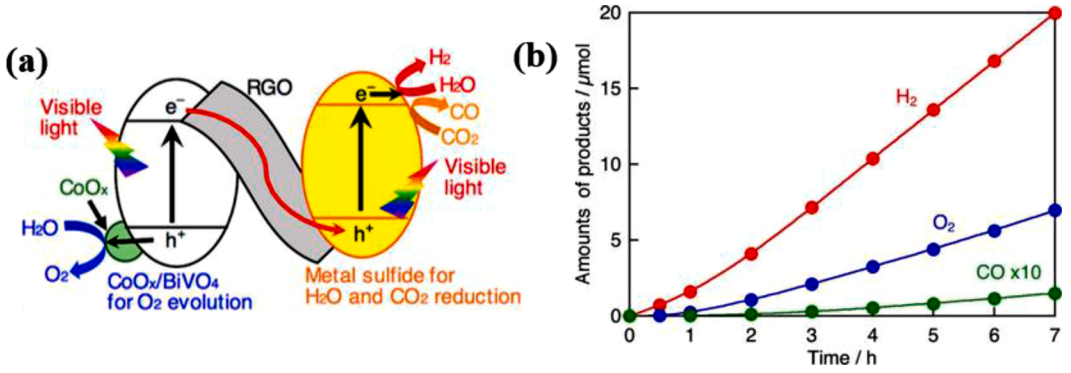

Fig. 7. (a) Z-scheme charge transfer of the CoO_x-RGO/$BiVO_4$/$CuGaS_2$ semiconductor photocatalysts for water splitting and CO_2 photoreduction reaction; (b) Products evolution for CO_2 photocatalytic reduction reaction performed under visible light (λ>400 nm) using $CuGaS_2$ (0.05 g) and CoO_x-RGO/$BiVO_4$ (0.05 g) composite suspended in 120 mL of water [107].

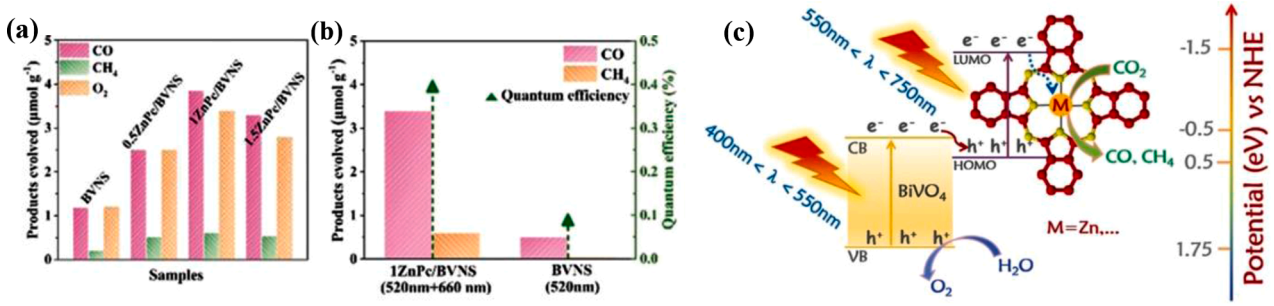

Fig. 8. (a) Photocatalytic activity for CO_2 reduction using xZnPc-$BiVO_4$ where x is the mass ratio ZnPc:$BiVO_4$. The reaction was performed under visible light (λ>420 nm) using 0.1 g of catalyst suspended in 5 mL of water for 4 hours.; (b) Quantum efficiency under monochromatic beams; (c) S-scheme configuration charge carrier transfer and separation proposed for ZnPc-coated $BiVO_4$ nanosheets [109].

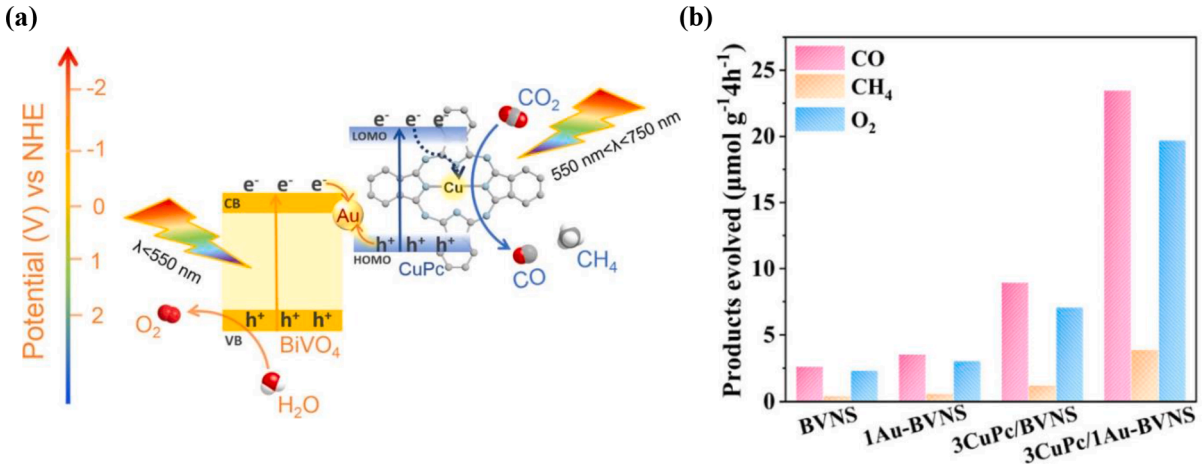

Fig. 9. (a) Z-scheme for charge carriers transfer and separation proposed for CuPc/Au-$BiVO_4$. (b) O_2, CH_4, and CO production of bare $BiVO_4$ nanosheets (BVNS) and xCuPc/yAu-BiNS, where x and y are the mass ratio percent of CuPc and Au, respectively [110].

using only Cu_2O, showing that the C layer avoids photooxidation of the Cu_2O NWA [97].

A similar system, with reduced graphene oxide (RGO) as electron mediator material, was proposed by Xiaona Li et al. [99], where a Cu_2O-RGO/$BiVO_4$ all-solid-state Z-scheme was constructed and showed improved CO_2 conversion with concurrent benzyl alcohol oxidation. The Cu_2O-RGO/$BiVO_4$ was prepared via thermal annealing of Cu precursor in the presence of previously prepared RGO/$BiVO_4$. The bare Cu_2O produced about ~0.05 μmol of HCOOH, 0.06 μmol of H_2, and 0.13 μmol of benzaldehyde after 24 h of simulated solar light irradiation. In contrast, Cu_2O-RGO/$BiVO_4$ showed higher conversion to HCOOH (0.65 μmol), H_2 (0.73 μmol), and benzaldehyde (2.16 μmol). According to the authors, the Cu_2O-RGO/$BiVO_4$ nanocomposite showed better photocatalytic performance due to the Z-scheme charge transfer pathway formed, facilitating the electron transfer from $BiVO_4$ CB to Cu_2O VB, with RGO acting as an electron mediator [99]. As discussed before [97], the Z-scheme stabilized Cu_2O against photocorrosion, and the system presented no evident decrease in photoactivity.

A novel $BiVO_4$/$Cu_{0.4}V_2O_5$ direct Z-scheme (S-scheme) catalyst was fabricated by growing $Cu_{0.4}V_2O_5$ nanosheets on the surface of $BiVO_4$ microplates using a simple co-precipitation process. Briefly, the $BiVO_4$ (0.5 mmol) microplates were dispersed in different concentrations of Cu $(NO_3)_3.3H_2O$ (20 mL) to form a mixture after a sonication process. Further, $Na_3VO_4.12H_2O$ aqueous solution was added to the above mixture, stirred at room temperature, and then centrifuged to collect the powder. Then powder was washed and dried to form $BiVO_4$/$Cu_{0.4}V_2O_5$ composites [100]. The photocatalytic performance of $BiVO_4$/$Cu_{0.4}V_2O_5$ composites for CO_2 reduction was evaluated under light irradiation at 160 mW·cm^{-2} (420 – 780 nm). For pristine $BiVO_4$, only trace amounts of CO were detected, indicating that $BiVO_4$ was not active in the photocatalytic conversion of CO_2 to CO. In contrast, pristine $Cu_{0.4}V_2O_5$ produced 2.18 μmol g^{-1} h^{-1} of CO. When both materials were combined to form the S-scheme heterojunction, about 4.4 times more CO was obtained compared to only $Cu_{0.4}V_2O_5$, demonstrating its advantage for CO_2 to CO conversion. The authors concluded that charge migration in $BiVO_4$/$Cu_{0.4}V_2O_5$ occurs by transferring photoinduced electrons from $BiVO_4$ CB to $Cu_{0.4}V_2O_5$ VB with subsequent recombination with the holes therein present. It would lead accumulation of photoinduced electrons with strong reduction potential in the $Cu_{0.4}V_2O_5$ CB and holes with high positive oxidation potential in $BiVO_4$ VB. Finally, the photoexcited electrons in the $Cu_{0.4}V_2O_5$ CB would realize the reduction of CO_2 to CO (Fig. 5c) [100].

A Z-scheme bias-free PEC artificial leaf employing an enzyme semiconductor photobiocathode was recently reported [101]. For this, the authors used FeOOH/$BiVO_4$ as n-type photoanode and TiO_2-coated $CuFeO_2$/CuO (CFO)/*Clostridium Ljungdahlii* formate dehydrogenase (ClFDH) as p-type biohybrid photocathode. The $BiVO_4$ was prepared by the electrodeposition method on an FTO substrate, and then the FeOOH oxygen-evolution catalyst was deposited through photoelectrodeposition in $(NH_4)_2Fe(SO_4)_2{\cdot}6H_2O$ (0.1 M) aqueous solution. The FeOOH|$BiVO_4$ photoanode with 1 cm × 1 cm was connected to a ClFDH-TiO_2|CFO photobiocathode (1 cm × 1 cm) using copper tape. Then, the edges of the FeOOH|$BiVO_4$||ClFDH-TiO_2|CFO device were covered with epoxy resin to securely anchor these two photoelectrodes. The central idea was to transfer the photoexcited electrons from CFO to ClFDH. Biocatalytic PEC conversion of CO_2 to formate was performed in a chamber containing CO_2 saturated phosphate butter (pH 6.5, 50 mM bicarbonate). A three-electrode system was used with ClFDH-TiO_2|CFO

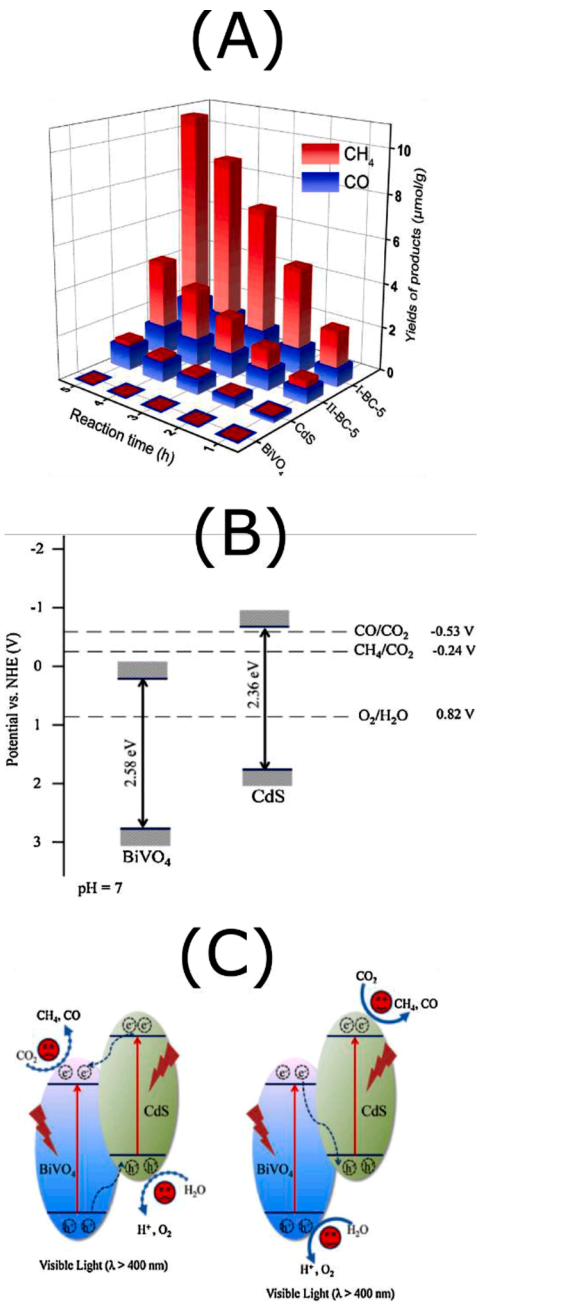

Fig. 10. (a) Yields of CH_4 and CO where I-BC-5 and II-BC-5 represent 15-30 nm and 55-75 nm thick CdS/$BiVO_4$ composites containing 31.3 and 30,7 % of CdS, respectively. The reaction was performed under a batch regimen at 3 Bar and using visible light (λ>420 nm) at 145.9 mW/cm^2, using 20 mg of the photocatalyst in contact directly with CO_2 and water vapor. (b) Band positions for $BiVO_4$ and CdS vs. NHE. (c) Type II heterojunction mechanism and (d) proposed S-scheme mechanism [46].

as the working electrode, Ag/AgCl as the reference electrode, and graphite as the counter electrode, while a two-electrode configuration was used with a FeOOH|$BiVO_4$ as working electrode and a ClFDH-TiO_2|CFO as counter electrode. The chamber was irradiated with a Xe lamp (100 mW/cm^2, 420 < λ < 900 nm). As a result, the FeOOH/$BiVO_4$|ClFDH-TiO_2/CFO tandem PEC cell produced formate at a rate of 0.098 μmol h^{-1} cm^{-2} (solar-to-formate conversion efficiency of 0.008%), which was 2.45 and 4.90 times higher than those of FeOOH/$BiVO_4$|TiO_2/CFO and FeOOH/$BiVO_4$|CFO, respectively. The authors proposed a mechanism where the photoanode consumed photoexcited holes to oxidize water, transferring the photoexcited electrons to CFO VB. The photoexcited electrons in CFO transferred to ClFDH/TiO_2 for unbiased CO_2 reduction (Fig. 5d) [101].

Recently reported, an all-solid-state Z-scheme sandwiched structure of $Cd_xZn_{1-x}S$@Au deposited on (010) $BiVO_4$ facets, where Au act as a solid electron mediator, was investigated [102]. $BiVO_4$ was synthesized by a simple hydrothermal route and Au/$BiVO_4$ was synthesized using the photodeposition method using $AuCl_4.4H_2O$ as the precursor. Cd_xZn_{1-x} was coated on Au nanoparticles surface of Au/$BiVO_4$ by deposition precipitation method. Au acted as a carrier mediator to promote the electrons from $BiVO_4$ CB to $Cd_xZn_{1-x}S$ VB, leaving the light excited electrons in the $Cd_xZn_{1-x}S$ CB and the photoholes in the $BiVO_4$ VB. The system showed notable improvement in CO_2 reducing activity for the Z-scheme composite photocatalysts, and the highest rate of CO formation was 2.2 μmol g^{-1} h^{-1} for $Cd_{0.5}Zn_{0.5}S$@Au/$BiVO_4$. They explain the outstanding performance by synergistic effects from Schottky junction formation between $BiVO_4$ (010) and Au, Z-scheme mechanism, and doping effect (Fig. 5e).

A work using quinacridone (QA)/$BiVO_4$ nanocomposite prepared via directed QA self-assembly on hydroxylated $BiVO_4$ nanosheets was reported for CO_2 photoreduction [103]. $BiVO_4$ nanosheets were synthesized via a hydrothermal process using the $BiCl_3$, cetyltrimethylammonium bromide (CTAB), and $NaVO_3$ precursors heated in an autoclave at 120 °C for 8 h. The obtained powder was post-heat-treated at 400 °C for 8 min. Further, $BiVO_4$ nanosheets were mixed within a QA solution in dimethyl sulfoxide and stirred for 1 h. After drying, the morphology of the QA/$BiVO_4$ was the same as that of $BiVO_4$ nanosheets. The as-prepared pure $BiVO_4$ nanosheets and QA particles showed meager CO production rates of 1 and 17 μmol g^{-1} h^{-1}, respectively, while QA/$BiVO_4$ S-scheme heterojunction under optimized conditions produced 407 μmol g^{-1} h^{-1}. S-scheme formation enhanced the promotion and separation of charges between the two compounds so that the photogenerated electrons in the $BiVO_4$ CB quickly recombined with the photoinduced holes in the highest occupied molecular orbital of QA (Fig. 5f). Thus, spatially separated electrons in QA and holes in $BiVO_4$ would provide enough potential for CO_2 reduction [103].

Ji Bian et al. [104] designed an original cascade (001) TiO_2-g-C_3N_4/$BiVO_4$ S-scheme. The $BiVO_4$ nanosheets were synthesized as reported in the above case [103]. Then, C_3N_4 nanosheets were synthesized by a hydrothermal process, followed by post-annealing at 500 °C for 2 h. For the synthesis of (001) faced exposed anatase TiO_2 nanosheets, $Ti(OBu)_4$, absolute ethanol, and hydrofluoric acid were mixed and hydrothermally treated at 160°C for 24 h. Different weight percentages of g-C_3N_4 and TiO_2 were investigated for CO_2 reduction, and the best results were found for 15 and 5 wt.% of g-C_3N_4 and (001) TiO_2, respectively. The final optimized system showed 60 μmol g^{-1} of CO after 4 hours with less CH_4 and O_2 from water oxidation half-reaction (under whole Xe spectrum irradiation). The authors proposed that higher activity comes from accelerated and maximized charge transfer by fabricating tightly connected interfaces and by timely transferring of photogenerated electrons from g-C_3N_4 to the introduced additional energy platform, impeding the electron accumulation in the CB of g-C_3N_4 and prolonging the lifetime of photogenerated electrons, as shown in Fig. 6a [104].

Mengfei Lu et al. proposed a similar S-scheme g-C_3N_4/$BiVO_4$ by a set of 2D/2D coupling of g-C_3N_4 and $BiVO_4$ ultrathin nanosheets via a thermal-polymerization and subsequent hydrothermal method [105]. First, the yellow sponge-like g-C_3N_4 nanosheets morphology was obtained by heating $C_2H_4N_4$ and NH_4C in a ratio of 1:10 at 500°C for 4 h. Further, g-C_3N_4 nanosheets were added to a mixture of $BiCl_3$, CTAB, and $NaVO_3$ precursors and solvothermal treated at 160 °C for 3 h. The g-C_3N_4/$BiVO_4$ with 2D ultrathin nanosheets morphology was obtained after pulverizing the final products. The heterostructures showed CH_4 and CO evolutions of 4.57 and 5.19 μmol g^{-1} h^{-1}, respectively, which were 4.8 and 4.4 times higher than the gaseous products evolved for pure g-C_3N_4. The improved CO_2 reduction was explained by faster charge transfer and separation related to the face-to-face 2D/2D

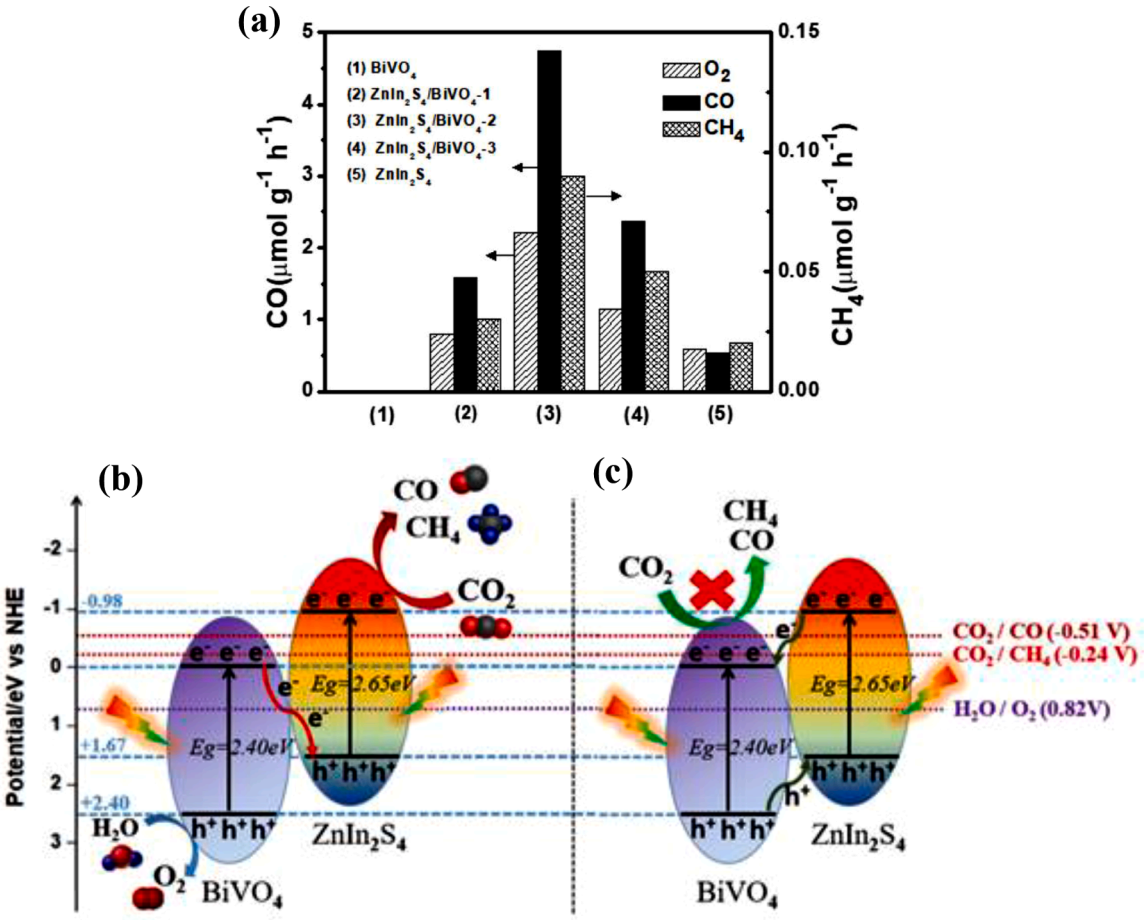

Fig. 11. (a) O_2, CO, and CH_4 evolution for $ZnIn_2S_4/BiVO_4$ using 0.1 g of as-prepared photocatalyst spread on the bottom of the batch reactor under 300 W Xenon lamp simulated sunlight and ambient pressure. $ZnIn_2S_4/BiVO_4$ composite materials were denoted as $ZnIn_2S_4/BiVO_4$-1, $ZnIn_2S_4/BiVO_4$-2, $ZnIn_2S_4/BiVO_4$-3 reflecting their different mole ratios of 0.02:1, 0.1:1 and 0.3:1, respectively. (b) S-scheme charge carriers mechanism and representation of photocatalytic reactions, and (c) discarded type-II heterojunction electron-transfer mechanism [111].

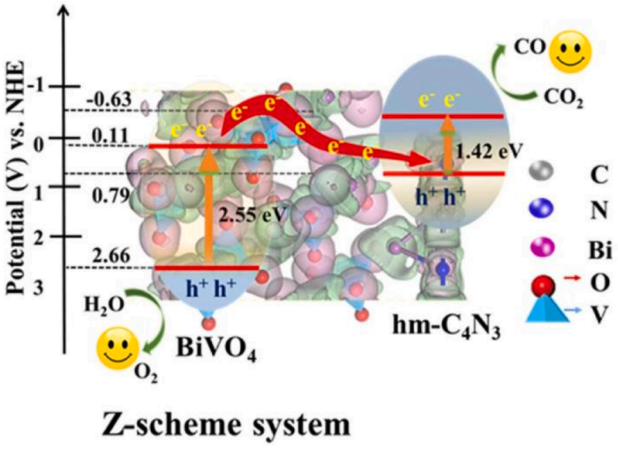

Fig. 12. S-scheme charge transfer mechanisms for $BiVO_4$/hm-C_4N_3 photocatalysts [112].

ultrathin nanosheets and S-scheme (Fig. 6b). From a thermodynamic point of view, it is important to highlight that photogenerated electrons in the g-C_3N_4 CB have enough driven force to reduce CO_2 since they are at more negative potentials than the potential of CO_2/CH_4 (-0.24 eV vs. NHE) [105].

A recently investigated ternary g-C_3N_4/Bi/$BiVO_4$ hybrid material was fabricated by pre-formed g-C_3N_4 nanosheets-mediated chemical deposition of $BiVO_4$ nanoparticles [106]. The g-C_3N_4 nanosheets were synthesized by directly heating melamine at 550°C for 4h. The entire product was ground and again heated at 550°C for 2 h to obtain g-C_3N_4 nanosheets. The binary g-C_3N_4/$BiVO_4$ nanocomposites were obtained by dissolving the g-C_3N_4 nanosheets in water and adding $Bi(NO_3)_3.5H_2O$ and NH_4VO_3 (1:1 ratio). After centrifugation, cleaning, and drying, the solid products were heated at 400 °C for 2 h to obtain the binary g-C_3N_4/$BiVO_4$ nanocomposites. Further, the g-C_3N_4/$BiVO_4$ nanocomposites were mixed in a dilute solution of $NaBH_4$, and the final ternary g-C_3N_4/Bi/$BiVO_4$ obtained by the *in-situ* reduction method was collected through centrifugation followed by washing and drying (50 °C for 12 h). The photocatalytic activity was investigated by CO_2 reduction and oxidation of water vapor, and the presence of Bi NPs significantly increased the photocatalytic performance for CO formation. The mechanism proposed by the authors is represented in Fig. 6c, which includes three active visible-light absorption centers (g-C_3N_4 nanosheets, $BiVO_4$, and Bi NPs). The metallic Bi NPs additionally acted as electron mediators to promote the interfacial charge transfer in the hybrid system. The charge recombination was inhibited by transferring photoexcited electrons from Bi NPs to $BiVO_4$ CB and then toward g-C_3N_4 VB. Consequently, holes in g-C_3N_4 VB and electrons in $BiVO_4$ CB with low redox capacity are sacrificed, while electrons in g-C_3N_4 CB and holes in $BiVO_4$ VB, presenting higher redox capacities, remain at their sites and are more efficiently separated. The mentioned processes modulate the dynamics to suit both aerobic photocatalytic oxidation and

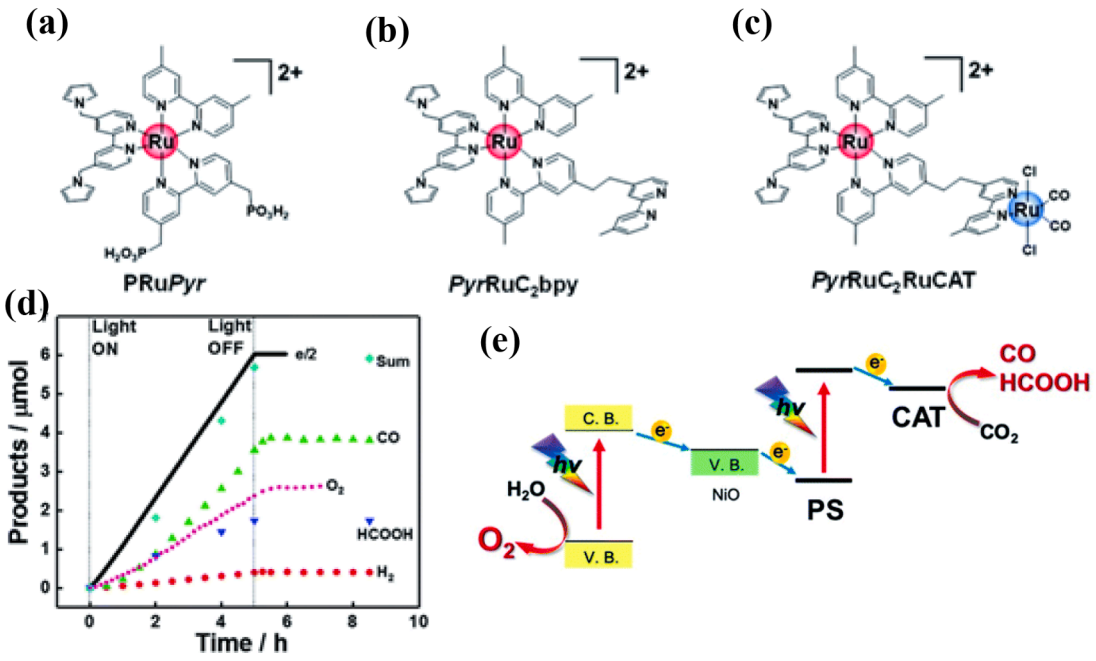

Fig. 13. (a,b,c) Ruthenium complexes for sensitizing and catalytic center. (d) Gaseous products obtained under visible light and zero bias in a PEC two-photoelectrode device (NiO/PRu-PolyPyr-RuC2RuCAT1 photocathode: 460 – 650 nm, 32 mW cm^{-2}; CoOx/$BiVO_4$ photoanode: 400 – 650 nm, 28 mW cm^{-2}). (e) Proposed Z-scheme charge transfer mechanisms for NiO/PRu-PolyPyr-RuC_2RuCAT and related reactions [113].

anaerobic photocatalytic reduction reactions [106].

Kudo *et al.* [107] reported a powdered all-solid-state Z-scheme setup, where the obtained CoO_x-RGO/$BiVO_4$ was dispersed in a $CuGaS_2$ suspension to carry out water splitting and CO_2 photoreduction reactions under visible-light irradiation. CoO_x-RGO/$BiVO_4$ was synthesized by adding $Co(NO_3)$ to the $BiVO_4$ prepared by solid-state reaction and the obtained powder was further annealed to obtain CoO_x/$BiVO_4$. Next, CoO_x-RGO/$BiVO_4$ composites were obtained by dispersing CoO_x/$BiVO_4$ in methanol (50 vol.%) and light irradiating the system for 3 h. CoO_x cocatalysts contributed to increasing O_2 evolution while RGO mediated electron transfer from $BiVO_4$ CB to $CuGaS_2$ VB, suppressing charge recombination (Fig. 7a). CO_2 photoreduction yielded ~20 nmol g^{-1} of CO and 20 µmol g^{-1} of H_2 after irradiating the suspension for 7 hours in pure water, without hole scavengers, as shown in Fig. 7b. Although $CuGaS_2$ CB is suitable to promote CO_2 reduction, the water reduction was three orders of magnitude higher, where the multiple steps required for CO_2 photoreduction might be a factor that favors the water reduction. Besides the low selectivity to CO generation, the CO_2 reduction reaction is performed through interparticle charge carrier transfer, opening opportunities for the design of new hybrid powdered Z-scheme systems [107].

The interparticle charge transfer was also used to establish a direct Z-scheme configuration between Rh-doped $SrTiO_3$ prepared by the solid-state reaction method and monoclinic $BiVO_4$ powders separately dispersed in water [108]. In the synthesis process of Rh-doped $SrTiO_3$; starting products, i.e. $SrCO_3$, Rh_2O_3, and TiO_2 are mixed and the mixture is calcined at 1173 K for 1 h. Then, the powder is post-heat-treated at 1273-1373 K for 10 h to obtain Rh-doped $SrTiO_3$ particles. This S-scheme configuration ($BiVO_4$ and $SrTiO_3$:Rh) was active to convert CO_2 to CO at a rate of 0.018 µmol h^{-1} and split water to H_2 and O_2 at 8.7 and 4.0 µmol h^{-1}, respectively, under visible light irradiation. The CO conversion increased up to 1.8 times through introducing metallic co-catalysts to $SrTiO_3$:Rh, and CO production rate and selectivity were found to be modulated by the cocatalyst size, suggesting that the smaller particles lead to a rise in conversion and selectivity [84]. No products were detected when bare $SrTiO_3$: Rh or $BiVO_4$ were adopted alone as photocatalysts. Although the work shows an interesting powdered photocatalyst system with interparticle charge transfer, the selectivity of CO is below 1%, and several modifications are still necessary.

Besides semiconductors, molecular components can also construct Z-scheme heterojunctions, as exemplified by Jing *et al.* [109]. The authors deposited a Zn phthalocyanine (ZnPc) on monoclinic $BiVO_4$ nanosheets generating an 8 nm thin ZnPc/$BiVO_4$ composite. The ZnPc/$BiVO_4$ composite was synthesized by a one-pot self-assembly method, where the ZnPc was dissolved in ethanol and mixed with the precursors of $BiVO_4$ ($BiCl_3$, CTAB, ethylene glycol, and $NaVO_3$). The composite product was obtained by a solvothermal process at 120°C for 12 h and the final powder calcinated at 400°C for 8 min. The obtained morphology of the ZnPc/$BiVO_4$ composite was similar to that of $BiVO_4$ nanosheets but with increased thickness compared to pristine sheets. Under CO_2 reduction and visible-light irradiation conditions for 4 hours, the ZnPc/$BiVO_4$ nanosheets showed CO and O_2 evolution of ~3.8 and ~3.4 µmol g^{-1}, respectively (Fig. 8a) [109]. Quantum efficiency for CO_2 photoreduction reaction increased 4 times after introducing ZnPc (Fig. 8b). Vibrational spectroscopy experiments indicated a strong interaction between ZnPc and $BiVO_4$, as suggested by V-O bond strength and weakened surface hydroxyl vibrational intensity with the introduction of ZnPc. This latter suppresses charge recombination as suggested by photoemission intensity increasing compared to bare $BiVO_4$ nanosheets. The combination of results indicated that the charge transfer occurs strictly when both ZnPc and $BiVO_4$ are excited simultaneously, implying that electron transfer from nanosheets CB to ZnPc HOMO, evidencing an S-scheme configuration as shown in Fig. 8c. The synergistic effects between $BiVO_4$ and the complex in the S-scheme arrangement and morphologic characteristics of $BiVO_4$ nanosheets were considered crucial factors to the CO_2 reduction achievement [109].

As aforementioned, the ZnPc interacts strongly with $BiVO_4$ nanosheets through hydroxyl groups on the surface, and this correlation is a central factor to keep a high charge carrier transfer [109]. The same research group developed a strategy involving Au NPs-oriented modulation of Cu phthalocyanine (CuPc) dispersity on the $BiVO_4$ nanosheets photocatalyst [110]. CuPc showed a robust interfacial interaction with Au NPs to accept photogenerated electrons from $BiVO_4$, according to the proposed all-solid-state Z-scheme mechanism (Fig. 9a). The CO_2 photoreduction products were CO and CH_4 with ~23 and ~3 µmol g^{-1} after 4h of reaction (equivalent to 5.75 and 0.75 µmol g^{-1} h^{-1}),

Table 2
Comparison of product evolution rates from CO_2 reduction using $BiVO_4$-based Z/S-schemed photocatalysts under different light illumination conditions.

Photocatalyst	Light source	CO_2 photoreduction Products	Evolution rate (μmol g^{-1} h^{-1})	Ref
Cu_2O-based				
$BiVO_4${010}-Au-Cu_2O	300 W Xe/ 420 nm filter*	CO, CH_4	2.08, 3.15	[98]
BVO/C/Cu_2O	300 W Xe/ 420 nm filter (100 mW cm^{-2})	CO	3.01	[97]
Cu_2O-RGO/$BiVO_4$	300 W Xe/ 420 nm filter*	HCOOH, H_2	0.027, 0.031[#]	[99]
C_3N_4-based				
(001)TiO_2-g-C_3N_4/ $BiVO_4$	300 W Xe/ 420 nm filter*	CO, CH_4	15.2, 0.5	[104]
g-C_3N_4/$BiVO_4$	300 W Xe/ 420 nm filter*	CO, CH_4	5.19, 4.57	[105]
g-C_3N_4/Bi/$BiVO_4$	300 W Xe/ 420 nm filter*	CO	1.3	[106]
$BiVO_4$/hm-C_4N_3	300 W Xe*	CO, CH_4	40.8, 2	[112]
Metal sulfide-based				
CdS/$BiVO_4$	300 W Xe /420 nm filter (145.9 mW cm^{-2})	CO, CH_4	0.39, 1.75	[46]
$Cd_{0.5}Zn_{0.5}S$@Au/ $BiVO_4$	300 W Xe/ 420 nm filter*	CO	2.2	[102]
$ZnIn_2S_4$/$BiVO_4$	300 W Xe*	CO, CH_4	4.75, 0.082	[111]
$CuGaS_2$ CoO_x-RGO/ $BiVO_4$	300 W Xe /420 nm filter (100 mW cm^{-2})	CO	0.0014	[107]
Phthalocyanine-based				
ZnPc/$BiVO_4$	300 W Xe /420 nm filter*	CO, CH_4	0.95, 0.15	[109]
CuPc/Au-$BiVO_4$	300 W Xe /420 nm filter*	CO, CH_4	5.75, 0.75	[110]
Others				
QA/10$BiVO_4$	300 W Xe/ 420 nm filter*	CO	407	[103]
Au-$SrTiO_3$:Rh/ $BiVO_4$	300 W Xe/ 350 nm filter*	CO	0.033[#]	[108]
NiO/PRu-PolyPyr-RuC_2RuCAT/ $BiVO_4$	300 W Xe /460 nm filter /(~30 mW cm^{-2})[†]	CO, HCOOH	0.78, 0.36[#]	[113]

* Irradiance not given.
[#] Units of μmol h^{-1}.
[†] photocathode (2 cm^2), and photoanode 1.2-2 cm^2).

respectively, accompanied by a considerable O_2 evolving as the water oxidation product [110]. Au-mediated CuPc/$BiVO_4$ Z-scheme approach improved 9- and 3-times the CO production compared to pristine $BiVO_4$ nanosheets and weakly dispersed CuPc/$BiVO_4$, respectively (Fig. 9b).

Li *et al.* [46] studied 15-30 nm and 55-75 nm thick monoclinic $BiVO_4$ nanosheets to explore the effect of shortening the charge carrier's diffusion length. $BiVO_4$ nanosheets were prepared through a solvothermal route and treated with Cd and thiourea, giving rise to CdS/$BiVO_4$ nanocomposites as CO_2 photoreduction catalysts. $BiVO_4$ nanosheets were synthesized by the hydrothermal method at 160°C for 2 h by using $Bi(NO_3)_3{\cdot}5H_2O$, $C_{18}H_{29}NaO_3S$, HNO_3, NH_4VO_3, and NaOH precursors. For obtention of CdS/$BiVO_4$ nanocomposites, the $BiVO_4$ nanosheets were added to a water solution containing $(CH_3COO)_2{\cdot}2H_2O$ and thiourea, stirred, and heated at 90°C for 2.5 h. The mixed morphology of the CdS/$BiVO_4$ nanocomposites was obtained, where CdS were nanoparticles dispersed on $BiVO_4$ nanosheets. The composite could produce either CH_4 or CO under batch conditions, under a CO_2 pressure of 3 bar, water vapor, and visible light irradiation. Fig. 10a shows that thinner $BiVO_4$ nanosheets (I-BC-5 sample) produced higher conversions of 8.73 and 1.95 μmol g^{-1} of CH_4 and CO, respectively, after 5 h irradiation. This enhancement follows the decrease of the charge carrier path to the particle's surface, improving charge separation. Moreover, the authors correlate the availability of electrons on the surface with the selectivity of the reaction, highlighting that the yield of CH_4 was higher using composites based on thinner $BiVO_4$ particles [46]. Considering that CO_2 to CH_4 and CO reduction reaction require 8 and 2 electrons, respectively, CO formation is favorable under deficient electron availability, shifting the selectivity of the reaction toward CO in the case of high charge recombination rates provided by thicker sheets. As shown in Fig. 10b, the S-scheme mechanism is further experimentally endorsed through electrons from CdS' CB because of its more positive potential than the minimum required for $O_2/O_2^{-\bullet}$ reaction (-0.046 eV vs. NHE). These observations were essential to elucidate the S-scheme mechanism of CdS/$BiVO_4$ heterojunction and helped explain the CO_2 photoreduction on the composite's surface, which would not be reasonable through type II heterojunction mechanism (Fig. 10c and 10d) [46].

Increasing the degree of dispersion of the material responsible for the CO_2 adsorption has also been a strategy to achieve a high surface area and enhance the availability of active sites for CO_2 photoreduction. Recently, Zou *et al.* studied $ZnIn_2S_4$ nanosheets grown on solvothermal-prepared $BiVO_4$ to create $ZnIn_2S_4$/$BiVO_4$ hierarchical heterostructures for CO and CH_4 production [111]. The synthesis of $ZnIn_2S_4$/$BiVO_4$ hierarchical heterostructures has followed several steps; in the first step $BiVO_4$ with a decahedron shape was synthesized by a hydrothermal process at 180°C for 12 h using the precursors $Bi(NO_3)_3{\cdot}5H_2O$, NH_4VO_3, and nitric acid. The as-prepared $BiVO_4$ powder was added to the mixture made by $ZnCl_2$, $InCl_3{\cdot}4H_2O$, and thioacetamide (TAA) in ethylene glycol, and heated at 90°C for 2 h. The bottom sediments were collected via filtration to obtain $ZnIn_2S_4$/$BiVO_4$. The $ZnIn_2S_4$ nanosheets were obtained using the above procedure without adding the $BiVO_4$. As shown in Fig. 11a, the obtained CO_2 reduction was affected by the loading content, exhibiting optimal CO production of 4.75 μmol g^{-1} h^{-1} and CH_4 production of 82 nmol g^{-1} h^{-1} when the $ZnIn_2S_4$:$BiVO_4$ ratio was 0.1:1. Since $BiVO_4$ CB is not negative enough, the type II heterojunction configuration was discarded (Fig. 11c), and a typical S-scheme mechanism was proposed (Fig. 11b) and further verified by calculations [111].

Exploring the efficient charges separation characteristics provided by spin-forbidden transitions of half-metallic C_4N_3 (hm-C_4N_3), Zou *et al.* applied this material as a cocatalyst for CO_2 photoreduction using $BiVO_4$/hm-C_4N_3 under S-scheme configuration [112]. Erythroid-like $BiVO_4$ was prepared by an elaborate combination of coprecipitation, template inducement, and hydrothermal technique. The $BiVO_4$/hm-C_4N_3 hybrid was fabricated through in-situ polymerization of $BMIm.C(CN)_3$ ionic liquids on $BiVO_4$, where ethyl acetate was mixed with $BMIm.C(CN)_3$ and then added to the already prepared $BiVO_4$, followed by ultrasonication. After the removal of ethyl acetate, the remaining products were annealed at 400°C to obtain $BiVO_4$/hm-C_4N_3 with flower-like (assembled from nanoparticles) morphology. Solvothermal-prepared erythroid-like $BiVO_4$ particles were coated by hm-C_4N_3 using an *in situ* polymerization of ionic liquids. The $BiVO_4$/hm-C_4N_3 converted CO_2 and H_2O into CO, CH_4, and O_2 under visible light irradiation, presenting an outstanding 97% CO selectivity with an evolution rate of 40.8 μmol g^{-1} h^{-1}, accompanied by a low CH_4 evolution rate of ~2 μmol g^{-1} h^{-1}. Compared to bare hm-C_4N_3, the S-schemed photocatalyst (Fig. 12) showed a 6-fold higher photoactivity, and the authors assigned this performance to the prolonged lifetime of photogenerated electrons. Furthermore, through *in-situ* DRIFTS

experiments, the authors identified the *COOH dehydration as the rate-limiting step due to the prominent signal at 1558 cm^{-1} assigned to this intermediate. This consideration supports DFT calculations, which revealed a significant energy barrier of 1.87 eV for hm-C_4N_3. For $BiVO_4$/hm-C_4N_3, this value decreased to 0.67 eV, indicating that the heterojunction's S-scheme configuration enhances the photoreduction performance by dropping the energy requirements for the rate-limiting step [112].

Another interesting molecular approach to exploring the all-solid-state Z-scheme configuration is using Ru polypyridine complexes because they can be used as a photosensitizer, absorbing material, and charge transfer mediator. Ishitani *et al.* explored these features, achieving a PEC configuration with a CoOx-coated $BiVO_4$ electrode for CO_2 photocatalytic reduction at zero bias [113]. The photocathode comprises a PRuPyr (Fig. 13a) anchored to a NiO electrode. The obtained material was submitted to electropolymerization with Pyr-RuC_2bpy (Fig. 13b) to produce the polypyrrole polymerization. Finally, $Ru(CO)_2Cl_2$ was introduced to coordinate with bipyridine of Pyr-RuC_2bpy moieties (Fig. 13c), yielding a NiO sensitized by polypyridinic Ru complex with terminal $Ru(bpy)(CO)_2Cl_2$ as the active part of the photocathode (named as NiO/PRu-*PolyPyr*-RuC_2RuCAT) [113]. Unlike a conventional PEC system, the CoOx-modified $BiVO_4$ photoanode conducted the CO_2 photoreduction and water oxidation reactions concomitantly without an applied bias. Zero bias PEC activity of the photocathode and photoanode was tested in a two-compartment H-type cell setup with a Nafion membrane separating the cathodic and anodic compartments. The authors reported 3.9, 1.82, and 0.42 μmols of CO, HCOOH, and H_2, respectively, after 5 hours under visible light irradiation (photocathode: $\lambda_{ex} = 460–650$ nm, 32 mW cm^{-2}; photoanode: $\lambda_{ex} =$ 400–650 nm, 28 mW cm^{-2}). It indicates a faradaic efficiency of 99 and 89 % for photocathode and photoanode, respectively, and a selectivity of 93 % for CO_2 photocatalytic reaction against H_2 production [113]. Under full-cell conditions, the Z-scheme mechanism suggested is represented in Fig. 13d. The Ru(II) photosensitizer unit in the photocathode and $BiVO_4$ n-type semiconductor in the photoanode absorb visible light to generate charge carriers. The photogenerated electrons through the metal to ligand charge transfer (MLCT) process are transferred to RuC_2RuCAT to perform photoreduction. Meanwhile, the photogenerated holes in $BiVO_4$ VB are transferred to CoOx to oxidize water to O_2. With the consumption of the holes in $BiVO_4$ VB, the electrons trapped at the $BiVO_4$ CB are transferred to the photocathode through the external circuit, reducing the excited state of the photosensitizer again, keeping the charge available to carry out the photoreactions [113].

The Z-scheme electron transfer process repeat endlessly during light irradiation, paving the way for the two-electron reduction of CO_2 on the photocathode to deliver CO and HCOOH, and the four-electron and two-electron oxidation of water to give O_2 and H_2O_2, respectively, at the photoanode side. Table 2 summarizes the $BiVO_4$-based Z/S-scheme photocatalysts discussed in this review article, comparing the products obtained from the photocatalytic CO_2 reduction reactions, their evolution rates, and the illumination systems.

5. Critical Comments

Photocatalytic reduction of CO_2 has been recognized as one of the most important strategies to convert sunlight into energy and renewable fuels and chemicals. Nevertheless, engineering photocatalyst materials to absorb sunlight and efficiently convert CO_2 is by far a formidable challenge. Bismuth vanadate is one of the most exciting materials for converting CO_2 assisted by sunlight due to several fascinating features, including its narrow bandgap, high chemical and physical stability, high absorption efficiency in the visible range, and low toxicity.

Our review highlighted the most recent work from the last 5 years that applied the $BiVO_4$ material in a Z/S-scheme configuration for photocatalytic CO_2 conversion. Although the primary products of CO_2 conversion are CH_4 and CO, Z/S-scheme systems comprising $BiVO_4$ can convert CO_2 to large molecules such as HCOOH, formate, or C2+. However, some hurdles must be overcome before the photocatalytic process can produce valuable chemical products on a large scale using CO_2 from the industrial exhaust. To reach such a level of competitiveness, a comprehensive understanding of charge transfer mechanisms between semiconductor materials, as well as increased efficiency and selectivity, will continue to be required. Some alternatives to boost photocatalysts development are the implementation of several well-known strategies and the standardization of experimental protocols, such as those described below. Apart from the strategies listed, it is crucial to enhance the efficiency of photoreactors, including the utilization of solar concentrators and methods for separating powder catalysts in aqueous and gas-phase processes.

(i) First of all, light source, optical filters, and irradiance information are mandatory to compare results among their peers. As shown in Table 2, several reports do not provide the irradiance, making any reasonable comparison extremely difficult. Even though some of them report the apparent quantum yield of the materials, it is still important to share all the light source information.
(ii) Exploits elementary doping of semiconductor materials to manipulate energy band positions and increase active sites, as well as to narrow the bandgap, resulting in enhanced visible light absorption;
(iii) Investigation of cocatalysts in order to enhance charge separation, boost photochemical activity, and increase selectivity and the number of active sites;
(iv) Deposition of nanoparticles with plasmonic properties;
(v) Deposition of noble-metal single-atoms with high dispersion on the surface of the photocatalyst to increase the number of active sites.

6. Conclusions

This short review summarizes the fundamental principles and recent advances in using bismuth vanadate ($BiVO_4$) in a Z/S-scheme photocatalysts configuration to convert CO_2 into more valuable chemicals. $BiVO_4$ as the oxidation photocatalyst associated with a wide variety of reduction photocatalysts, including Cu_2O, CdS, $ZnIn_2S_4$, ZnPc, g-C_3N_4, $CuFeO_2$, and others, can be used to establish heterostructures with charge transfer under the Z/S-scheme configuration. These configurations significantly boost visible-light absorption, promoting charge separations for targeting the conversion of CO_2 molecules into different valuable products. We show that modified $BiVO_4$ has been extensively used for CO_2 photoreduction due to its excellent oxidation properties, with some notable examples including (i) g-C_3N_4/$BiVO_4$ S-scheme that produces either CH_4 or CO with a yield rate of 5.19 and 4.57 μmol g^{-1} h^{-1}, respectively; (ii) FeOOH/$BiVO_4$/TiO_2/CFO Z-scheme that convert CO_2 to formate; (iii) Cu_2O-RGO/$BiVO_4$ all-solid-state Z-scheme with a conversion of CO_2 to HCOOH at a yield rate of 0.027 μmol g^{-1} h^{-1}, among many other examples.

Declaration of competing interests

The authors declare that they have no known competing financial interests or personal relationships that could have appeared to influence the work reported in this paper.

Acknowledgment

We gratefully acknowledge the support of the RCGI – Research Centre for Greenhouse Gas Innovation, hosted by the University of São Paulo (USP) and sponsored by FAPESP – São Paulo Research Foundation (2014/50279-4 and 2020/15230-5) and Shell Brasil, and the strategic importance of the support given by ANP (Brazil's National Oil, Natural Gas, and Biofuels Agency) through the R&D levy regulation. We also

acknowledge the Brazilian National Council for Scientific and Technological Development (CNPq) for grants # 305794/2019-1 (RVG), # 306024/2019-5 (LMR), and # 313300/2020-8 (HW). This work was partially supported by the Coordenação de Aperfeiçoamento de Pessoal de Nível Superior—Brasil (CAPES)—Finance Code 001 and Capes-PrInt program (grants # 88881.311921/2018-01 and # 88887.311920/2018-00).

References

[1] S.R. Lingampalli, M.M. Ayyub, C.N.R. Rao, Recent progress in the photocatalytic reduction of carbon dioxide, ACS Omega 2 (2017) 2740–2748, https://doi.org/10.1021/ACSOMEGA.7B00721.
[2] J. Ran, M. Jaroniec, S.-Z. Qiao, J. Ran, S.-Z. Qiao, M. Jaroniec, -Z S Qiao, Cocatalysts in Semiconductor-based Photocatalytic CO2 Reduction: Achievements, Challenges, and Opportunities, 30, Wiley Online Libr, 2018, https://doi.org/10.1002/adma.201704649.
[3] S. Hennessey, P. Farràs, Production of solar chemicals: gaining selectivity with hybrid molecule/semiconductor assemblies, Chem. Commun. 54 (2018) 6662–6680, https://doi.org/10.1039/C8CC02487A.
[4] S.N. Habisreutinger, L. Schmidt-Mende, J.K. Stolarczyk, L. Schmidt-Mende, J. K. Stolarczyk, S.N. Habisreutinger, Photocatalytic reduction of CO2 on TiO2 and other semiconductors, Wiley Online Libr 52 (2013) 7372–7408, https://doi.org/10.1002/anie.201207199.
[5] V. Kumaravel, J. Bartlett, S.C. Pillai, Photoelectrochemical conversion of carbon dioxide (CO2) into fuels and value-added products, ACS Energy Lett 5 (2020) 486–519, https://doi.org/10.1021/acsenergylett.9b02585.
[6] S.S. Meryem, S. Nasreen, M. Siddique, R. Khan, An overview of the reaction conditions for an efficient photoconversion of CO2, Rev. Chem. Eng. 34 (2018) 409–425, https://doi.org/10.1515/revce-2016-0016.
[7] M.M.F. Hasan, L.M. Rossi, D.P. Debecker, K.C. Leonard, Z. Li, B.C.E. Makhubela, C. Zhao, A. Kleij, Can CO2 and renewable carbon be primary resources for sustainable fuels and chemicals? ACS Sustain. Chem. Eng. 9 (2021) 12427–12430, https://doi.org/10.1021/acssuschemeng.1c06008.
[8] S. Xie, Q. Zhang, G. Liu, Y. Wang, Photocatalytic and photoelectrocatalytic reduction of CO2 using heterogeneous catalysts with controlled nanostructures, Chem. Commun. 52 (2016) 35–59, https://doi.org/10.1039/C5CC07613G.
[9] B. Kumar, M. Llorente, J. Froehlich, T. Dang, A. Sathrum, C.P. Kubiak, Photochemical and photoelectrochemical reduction of CO 2, Annu. Rev. Phys. Chem. 63 (2012) 541–569, https://doi.org/10.1146/ANNUREV-PHYSCHEM-032511-143759.
[10] S. Dey, B.S. Naidu, C.N.R. Rao, Beneficial effects of substituting trivalent ions in the B-site of La 0.5 Sr 0.5 Mn 1−x A x O 3 (A = Al, Ga, Sc) on the thermochemical generation of CO and H 2 from CO 2 and H 2 O, Dalt. Trans. 45 (2016) 2430–2435, https://doi.org/10.1039/C5DT04822B.
[11] S. Nitopi, E. Bertheussen, S.B. Scott, X. Liu, A.K. Engstfeld, S. Horch, B. Seger, I.E. L. Stephens, K. Chan, C. Hahn, J.K. Nørskov, T.F. Jaramillo, I. Chorkendorff, Progress and perspectives of electrochemical CO2 reduction on copper in aqueous electrolyte, Chem. Rev. 119 (2019) 7610–7672, https://doi.org/10.1021/acs.chemrev.8b00705.
[12] Ž. Kovačič, B. Likozar, M. Huš, Photocatalytic CO2 reduction: a review of ab initio mechanism, kinetics, and multiscale modeling simulations, ACS Catal 10 (2020) 14984–15007, https://doi.org/10.1021/acscatal.0c02557.
[13] J. Albero, Y. Peng, H. García, Photocatalytic CO2 reduction to C2+ products, ACS Catal 10 (2020) 5734–5749, https://doi.org/10.1021/acscatal.0c00478.
[14] J. Fu, K. Jiang, X. Qiu, J. Yu, M. Liu, Product selectivity of photocatalytic CO2 reduction reactions, Mater. Today. 32 (2020) 222–243, https://doi.org/10.1016/j.mattod.2019.06.009.
[15] S. Chen, D. Huang, P. Xu, W. Xue, L. Lei, M. Cheng, R. Wang, X. Liu, R. Deng, Semiconductor-based photocatalysts for photocatalytic and photoelectrochemical water splitting: will we stop with photocorrosion? J. Mater. Chem. A. 8 (2020) 2286–2322, https://doi.org/10.1039/C9TA12799B.
[16] N. Zhang, R. Long, C. Gao, Y. Xiong, Recent progress on advanced design for photoelectrochemical reduction of CO2 to fuels, Sci. China Mater. 61 (2018) 771–805, https://doi.org/10.1007/S40843-017-9151-Y.
[17] N.S. Lewis, D.G. Nocera, Powering the planet: Chemical challenges in solar energy utilization, Proc. Natl. Acad. Sci 103 (2006) 15729–15735, https://doi.org/10.1073/pnas.0603395103.
[18] J. Wu, Y. Huang, W. Ye, Y. Li, J. Wu, Y. Huang, W. Ye, Y. Li, CO2 reduction: from the electrochemical to photochemical approach, Adv. Sci. (2017) 4, https://doi.org/10.1002/ADVS.201700194.
[19] B. Kumar, M. Llorente, J. Froehlich, T. Dang, A. Sathrum, C.P. Kubiak, Photochemical and photoelectrochemical reduction of CO 2, Annu. Rev. Phys. Chem. 63 (2012) 541–569, https://doi.org/10.1146/annurev-physchem-032511-143759.
[20] K. Li, B. Peng, T. Peng, Recent advances in heterogeneous photocatalytic CO 2 conversion to solar fuels, ACS Catal. 6 (2016) 7485–7527, https://doi.org/10.1021/acscatal.6b02089.
[21] X. Li, J. Wen, J. Low, Y. Fang, J. Yu, Design and fabrication of semiconductor photocatalyst for photocatalytic reduction of CO2 to solar fuel, Sci. China Mater. 57 (2014) 70–100, https://doi.org/10.1007/S40843-014-0003-1.
[22] W. Tu, Y. Zhou, Z. Zou, Photocatalytic conversion of CO 2 into renewable hydrocarbon fuels: state-of-the-art accomplishment, challenges, and prospects, Adv. Mater. 26 (2014) 4607–4626, https://doi.org/10.1002/adma.201400087.
[23] D. Kang, T.W. Kim, S.R. Kubota, A.C. Cardiel, H.G. Cha, K.S. Choi, Electrochemical synthesis of photoelectrodes and catalysts for use in solar water splitting, Chem. Rev. 115 (2015) 12839–12887, https://doi.org/10.1021/ACS.CHEMREV.5B00498.
[24] J.C. Wang, L. Zhang, W.X. Fang, J. Ren, Y.Y. Li, H.C. Yao, J.S. Wang, Z.J. Li, Enhanced photoreduction CO2 activity over direct Z-Scheme α-Fe2O3/Cu2O heterostructures under visible light irradiation, ACS Appl. Mater. Interfaces. 7 (2015) 8631–8639, https://doi.org/10.1021/ACSAMI.5B00822.
[25] L. Li, J. Yan, T. Wang, Z.-J. Zhao, J. Zhang, J. Gong, N. Guan, Sub-10 nm rutile titanium dioxide nanoparticles for efficient visible-light-driven photocatalytic hydrogen production, Nat. Commun. 6 (2015) 5881, https://doi.org/10.1038/ncomms6881.
[26] Z.U. Rehman, M. Bilal, J. Hou, F.K. Butt, J. Ahmad, S. Ali, A. Hussain, Photocatalytic CO2 reduction using TiO2-based photocatalysts and TiO2 Z-scheme heterojunction composites: a review, Molecules 27 (2022) 2069, https://doi.org/10.3390/molecules27072069.
[27] G. Zhang, Z. Wang, J. Wu, Construction of a Z-scheme heterojunction for high-efficiency visible-light-driven photocatalytic CO2reduction, Nanoscale 13 (2021) 4359–4389, https://doi.org/10.1039/d0nr08442e.
[28] J. Low, B. Cheng, J. Yu, Surface modification and enhanced photocatalytic CO2 reduction performance of TiO2: a review, Appl. Surf. Sci. 392 (2017) 658–686, https://doi.org/10.1016/j.apsusc.2016.09.093.
[29] X. Huang, W. Gu, Y. Ma, D. Liu, N. Ding, L. Zhou, J. Lei, L. Wang, J. Zhang, Recent advances of doped graphite carbon nitride for photocatalytic reduction of CO2: a review, Res. Chem. Intermed. 46 (2020) 5133–5164, https://doi.org/10.1007/s11164-020-04278-6.
[30] D. Cui, W. Hao, J. Chen, The synergistic effect of heteroatom doping and vacancy on the reduction of CO2 by photocatalysts, ChemNanoMat 7 (2021) 894–901, https://doi.org/10.1002/cnma.202100148.
[31] K. Xie, N. Umezawa, N. Zhang, P. Reunchan, Y. Zhang, J. Ye, Self-doped SrTiO3−δ photocatalyst with enhanced activity for artificial photosynthesis under visible light, Energy Environ. Sci. 4 (2011) 4211, https://doi.org/10.1039/c1ee01594j.
[32] V.P. Indrakanti, J.D. Kubicki, H.H. Schobert, Photoinduced activation of CO2 on Ti-based heterogeneous catalysts: current state, chemical physics-based insights and outlook, Energy Environ. Sci. 2 (2009) 745, https://doi.org/10.1039/b822176f.
[33] D. Jiang, W. Wang, E. Gao, S. Sun, L. Zhang, Highly selective defect-mediated photochemical CO2 conversion over fluorite ceria under ambient conditions, Chem. Commun. 50 (2014) 2005, https://doi.org/10.1039/c3cc47806h.
[34] K. Iizuka, T. Wato, Y. Miseki, K. Saito, A. Kudo, Photocatalytic reduction of carbon dioxide over Ag cocatalyst-loaded ALa4Ti4O15 (A = Ca, Sr, and Ba) using water as a reducing reagent, J. Am. Chem. Soc. 133 (2011) 20863–20868, https://doi.org/10.1021/ja207586e.
[35] D. Jiang, Y. Zhou, Q. Zhang, Q. Song, C. Zhou, X. Shi, D. Li, Synergistic integration of AuCu Co-catalyst with oxygen vacancies on TiO 2 for efficient photocatalytic conversion of CO 2 to CH 4, ACS Appl. Mater. Interfaces. 13 (2021) 46772–46782, https://doi.org/10.1021/acsami.1c14371.
[36] X. Li, J. Yu, M. Jaroniec, X. Chen, Cocatalysts for selective photoreduction of CO2 into solar fuels, Chem. Rev. 119 (2019) 3962–4179, https://doi.org/10.1021/acs.chemrev.8b00400.
[37] L. Ye, Y. Deng, L. Wang, H. Xie, F. Su, Bismuth-based photocatalysts for solar photocatalytic carbon dioxide conversion, ChemSusChem 12 (2019) 3671–3701, https://doi.org/10.1002/cssc.201901196.
[38] T.D.T.T. Nguyen, V.H.V.H. Nguyen, S. Nanda, D.V.N. Vo, V.H.V.H. Nguyen, T. Van Tran, L.X. Nong, T.D.T.T. Nguyen, L.G. Bach, B. Abdullah, S.S. Hong, T. Van Nguyen, BiVO4 photocatalysis design and applications to oxygen production and degradation of organic compounds: a review, Environ. Chem. Lett. 18 (2020) 1779–1801, https://doi.org/10.1007/S10311-020-01039-0.
[39] C.H. Claudino, M. Kuznetsova, B.S. Rodrigues, C. Chen, Z. Wang, M. Sardela, J. S. Souza, Facile one-pot microwave-assisted synthesis of tungsten-doped BiVO4/WO3 heterojunctions with enhanced photocatalytic activity, Mater. Res. Bull. 125 (2020), 110783, https://doi.org/10.1016/j.materresbull.2020.110783.
[40] K. Tolod, S. Hernández, N. Russo, Recent advances in the BiVO4 photocatalyst for sun-driven water oxidation: top-performing photoanodes and scale-up challenges, Catalysts 7 (2017) 13, https://doi.org/10.3390/catal7010013.
[41] L.E. Gomes, A.C. Nogueira, M.F. da Silva, L.F. Plaça, L.J.Q. Maia, R.V. Gonçalves, S. Ullah, S. Khan, H. Wender, Enhanced photocatalytic activity of BiVO4/Pt/PtOx photocatalyst: the role of Pt oxidation state, Appl. Surf. Sci. 567 (2021), 150773, https://doi.org/10.1016/j.apsusc.2021.150773.
[42] S. Ullah, A.A.Khan Fayeza, A. Jan, S.Q. Aain, E.P.F. Neto, Y.E. Serge-Correales, R. Parveen, H. Wender, U.P. Rodrigues-Filho, S.J.L. Ribeiro, Enhanced photoactivity of BiVO4/Ag/Ag2O Z-scheme photocatalyst for efficient environmental remediation under natural sunlight and low-cost LED illumination, Colloids Surfaces A Physicochem. Eng. Asp. 600 (2020), 124946, https://doi.org/10.1016/j.colsurfa.2020.124946.
[43] F. Deng, X. Lu, Y. Luo, J. Wang, W. Che, R. Yang, X. Luo, S. Luo, D.D. Dionysiou, Novel visible-light-driven direct Z-scheme CdS/CuInS2 nanoplates for excellent photocatalytic degradation performance and highly-efficient Cr(VI) reduction, Chem. Eng. J. 361 (2019) 1451–1461, https://doi.org/10.1016/j.cej.2018.10.176.

[44] B.D. Queiroz, J.A. Fernandes, C.A. Martins, H. Wender, Photocatalytic fuel cells: from batch to microfluidics, J. Environ. Chem. Eng. 10 (2022), 107611, https://doi.org/10.1016/j.jece.2022.107611.

[45] Y. Vasseghian, A. Khataee, E.N. Dragoi, M. Moradi, S. Nabavifard, G. Oliveri Conti, A. Mousavi Khaneghah, Pollutants degradation and power generation by photocatalytic fuel cells: a comprehensive review, Arab. J. Chem. 13 (2020) 8458–8480, https://doi.org/10.1016/j.arabjc.2020.07.016.

[46] Z.-H. Wei, Y.-F. Wang, Y.-Y. Li, L. Zhang, H.-C. Yao, Z.-J. Li, Enhanced photocatalytic CO2 reduction activity of Z-scheme CdS/BiVO4 nanocomposite with thinner BiVO4 nanosheets, J. CO2 Util. 28 (2018) 15–25, https://doi.org/10.1016/j.jcou.2018.09.008.

[47] T. Hisatomi, K. Domen, Progress in the demonstration and understanding of water splitting using particulate photocatalysts, Curr. Opin. Electrochem. 2 (2017) 148–154, https://doi.org/10.1016/j.coelec.2017.04.005.

[48] S. Shen, S.S. Mao, Nanostructure designs for effective solar-to-hydrogen conversion, Nanophotonics 1 (2012) 31–50, https://doi.org/10.1515/nanoph-2012-0010.

[49] F. Stelo, N. Kublik, S. Ullah, H. Wender, Recent advances in Bi2MoO6 based Z-scheme heterojunctions for photocatalytic degradation of pollutants, J. Alloys Compd. 829 (2020), 154591, https://doi.org/10.1016/j.jallcom.2020.154591.

[50] J.J. Concepcion, R.L. House, J.M. Papanikolas, T.J. Meyer, Chemical approaches to artificial photosynthesis, Proc. Natl. Acad. Sci 109 (2012) 15560–15564, https://doi.org/10.1073/pnas.1212254109.

[51] A.A. Khan, M. Tahir, Recent advancements in engineering approach towards design of photo-reactors for selective photocatalytic CO2 reduction to renewable fuels, J. CO2 Util. 29 (2019) 205–239, https://doi.org/10.1016/j.jcou.2018.12.008.

[52] C. Martinez Suarez, S. Hernández, N. Russo, BiVO4 as photocatalyst for solar fuels production through water splitting: a short review, Appl. Catal. A Gen. 504 (2015) 158–170, https://doi.org/10.1016/j.apcata.2014.11.044.

[53] J.L. White, M.F. Baruch, J.E. Pander, Y. Hu, I.C. Fortmeyer, J.E. Park, T. Zhang, K. Liao, J. Gu, Y. Yan, T.W. Shaw, E. Abelev, A.B. Bocarsly, Light-driven heterogeneous reduction of carbon dioxide: photocatalysts and photoelectrodes, Chem. Rev. 115 (2015) 12888–12935, https://doi.org/10.1021/acs.chemrev.5b00370.

[54] X. Wang, F. Wang, Y. Sang, H. Liu, X. Wang, F. Wang, Y. Sang, H. Liu, Full-spectrum solar-light-activated photocatalysts for light–chemical energy conversion, 7, Wiley Online Libr, 2017, https://doi.org/10.1002/aenm.201700473.

[55] S.G. Kumar, L.G. Devi, Review on modified TiO 2 photocatalysis under UV/visible light: selected results and related mechanisms on interfacial charge carrier transfer dynamics, J. Phys. Chem. A. 115 (2011) 13211–13241, https://doi.org/10.1021/jp204364a.

[56] N. Yang, J. Zhai, D. Wang, Y. Chen, L. Jiang, Two-dimensional graphene bridges enhanced photoinduced charge transport in dye-sensitized solar cells, ACS Nano 4 (2010) 887–894, https://doi.org/10.1021/NN901660V.

[57] L. Mu, Y. Zhao, A. Li, S. Wang, Z. Wang, J. Yang, Y. Wang, T. Liu, R. Chen, J. Zhu, F. Fan, R. Li, C. Li, Enhancing charge separation on high symmetry SrTiO 3 exposed with anisotropic facets for photocatalytic water splitting, Energy Environ. Sci. 9 (2016) 2463–2469, https://doi.org/10.1039/C6EE00526H.

[58] J. Albero, Y. Peng, H. García, Photocatalytic CO2 reduction to C2+ products, ACS Catal 10 (2020) 5734–5749, https://doi.org/10.1021/ACSCATAL.0C00478.

[59] P. Verma, F.A. Rahimi, D. Samanta, A. Kundu, J. Dasgupta, T.K. Maji, Visible-light-driven photocatalytic CO2 reduction to CO/CH4 using a metal–organic "soft" coordination polymer gel, Angew. Chemie - Int. Ed. (2022) 61, https://doi.org/10.1002/ANIE.202116094.

[60] S.S. Bhosale, A.K. Kharade, E. Jokar, A. Fathi, S.M. Chang, E.W.G. Diau, Mechanism of photocatalytic CO2 reduction by bismuth-based perovskite nanocrystals at the gas-solid interface, J. Am. Chem. Soc. 141 (2019) 20434–20442, https://doi.org/10.1021/JACS.9B11089.

[61] A. Ahmad Beigi, S. Fatemi, Z. Salehi, Synthesis of nanocomposite CdS/TiO2 and investigation of its photocatalytic activity for CO2 reduction to CO and CH4 under visible light irradiation, J. CO2 Util. 7 (2014) 23–29, https://doi.org/10.1016/j.jcou.2014.06.003.

[62] R.R. Ikreedeegh, M. Tahir, Indirect Z-scheme heterojunction of NH2-MIL-125(Ti) MOF/g-C3N4 nanocomposite with RGO solid electron mediator for efficient photocatalytic CO2 reduction to CO and CH4, J. Environ. Chem. Eng. 9 (2021), 105600, https://doi.org/10.1016/j.jece.2021.105600.

[63] S. Xie, W. Ma, X. Wu, H. Zhang, Q. Zhang, Y. Wang, Y. Wang, Photocatalytic and electrocatalytic transformations of C1 molecules involving C–C coupling, Energy Environ. Sci. 14 (2021) 37–89, https://doi.org/10.1039/D0EE01860K.

[64] Y. Ma, X. Wang, Y. Jia, X. Chen, H. Han, C. Li, Titanium dioxide-based nanomaterials for photocatalytic fuel generations, Chem. Rev. 114 (2014) 9987–10043, https://doi.org/10.1021/cr500008u.

[65] B. Parkinson, Advantages of solar hydrogen compared to direct carbon dioxide reduction for solar fuel production, ACS Energy Lett. 1 (2016) 1057–1059, https://doi.org/10.1021/acsenergylett.6b00377.

[66] S. Xie, Y. Wang, Q. Zhang, W. Deng, Y. Wang, MgO- and Pt-promoted TiO2 as an efficient photocatalyst for the preferential reduction of carbon dioxide in the presence of water, ACS Catal 4 (2014) 3644–3653, https://doi.org/10.1021/cs500648p.

[67] J. Ke, M. Adnan Younis, Y. Kong, H. Zhou, J. Liu, L. Lei, Y. Hou, Nanostructured ternary metal tungstate-based photocatalysts for environmental purification and solar water splitting: a review, Nano-Micro Lett. 10 (2018), https://doi.org/10.1007/S40820-018-0222-4.

[68] A. Navaee, A. Salimi, Specific anion effects on copper surface through electrochemical treatment: enhanced photoelectrochemical CO2 reduction activity of derived nanostructures induced by chaotropic anions, Appl. Surf. Sci. 440 (2018) 897–906, https://doi.org/10.1016/j.apsusc.2018.01.212.

[69] Y. Liu, B. Huang, Y. Dai, X. Zhang, X. Qin, M. Jiang, M.-H. Whangbo, Selective ethanol formation from photocatalytic reduction of carbon dioxide in water with BiVO4 photocatalyst, Catal. Commun. 11 (2009) 210–213, https://doi.org/10.1016/j.catcom.2009.10.010.

[70] J. Mao, T. Peng, X. Zhang, K. Li, L. Zan, Selective methanol production from photocatalytic reduction of CO2 on BiVO4 under visible light irradiation, Catal. Commun. 28 (2012) 38–41, https://doi.org/10.1016/j.catcom.2012.08.008.

[71] Y.J. Jang, J.-W. Jang, J. Lee, J.H. Kim, H. Kumagai, J. Lee, T. Minegishi, J. Kubota, K. Domen, J.S. Lee, Selective CO production by Au coupled ZnTe/ZnO in the photoelectrochemical CO 2 reduction system, Energy Environ. Sci. 8 (2015) 3597–3604, https://doi.org/10.1039/C5EE01445J.

[72] J.-W. Jang, S. Cho, G. Magesh, Y.J. Jang, J.Y. Kim, W.Y. Kim, J.K. Seo, S. Kim, K.-H. Lee, J.S. Lee, Aqueous-solution route to zinc telluride films for application to CO2 reduction, Angew. Chemie Int. Ed. 53 (2014) 5852–5857, https://doi.org/10.1002/anie.201310461.

[73] M. Schreier, P. Gao, M.T. Mayer, J. Luo, T. Moehl, M.K. Nazeeruddin, S.D. Tilley, M. Grätzel, Efficient and selective carbon dioxide reduction on low cost protected Cu 2 O photocathodes using a molecular catalyst, Energy Environ. Sci. 8 (2015) 855–861, https://doi.org/10.1039/C4EE03454F.

[74] J. Lin, Z. Pan, X. Wang, Photochemical reduction of CO2 by graphitic carbon nitride polymers, ACS Sustain. Chem. Eng. 2 (2014) 353–358, https://doi.org/10.1021/sc4004295.

[75] U. Kang, S.K. Choi, D.J. Ham, S.M. Ji, W. Choi, D.S. Han, A. Abdel-Wahab, H. Park, Photosynthesis of formate from CO2 and water at 1% energy efficiency via copper iron oxide catalysis, Energy Environ. Sci. 8 (2015) 2638–2643, https://doi.org/10.1039/C5EE01410G.

[76] G. Liao, C. Li, X. Li, B. Fang, Emerging polymeric carbon nitride Z-scheme systems for photocatalysis, Cell Reports Phys. Sci. 2 (2021), 100355, https://doi.org/10.1016/j.xcrp.2021.100355.

[77] J. Zhang, J. Yu, M. Jaroniec, J.R. Gong, Noble metal-free reduced graphene oxide-Zn x Cd 1− x S nanocomposite with enhanced solar photocatalytic H 2 -Production Performance, Nano Lett 12 (2012) 4584–4589, https://doi.org/10.1021/nl301831h.

[78] S.-I. In, D.D. Vaughn, R.E. Schaak, Hybrid CuO-TiO2−xNx hollow nanocubes for photocatalytic conversion of CO2 into methane under solar irradiation, Angew. Chemie Int. Ed. 51 (2012) 3915–3918, https://doi.org/10.1002/anie.201108936.

[79] H. Nakanishi, K. Iizuka, T. Takayama, A. Iwase, A. Kudo, Highly active NaTaO3-based photocatalysts for CO2 reduction to form CO using water as the electron donor, ChemSusChem 10 (2017) 112–118, https://doi.org/10.1002/CSSC.201601360.

[80] D.P. Acharya, N. Camillone, P. Sutter, CO 2 adsorption, diffusion, and electron-induced chemistry on rutile TiO 2 (110): a low-temperature scanning tunneling microscopy study, J. Phys. Chem. C. 115 (2011) 12095–12105, https://doi.org/10.1021/jp202476v.

[81] S.J.A. Moniz, S.A. Shevlin, D.J. Martin, Z.-X. Guo, J. Tang, Visible-light driven heterojunction photocatalysts for water splitting – a critical review, Energy Environ. Sci. 8 (2015) 731–759, https://doi.org/10.1039/C4EE03271C.

[82] H. Wang, L. Zhang, Z. Chen, J. Hu, S. Li, Z. Wang, J. Liu, X. Wang, Semiconductor heterojunction photocatalysts: design, construction, and photocatalytic performances, Chem. Soc. Rev. 43 (2014) 5234, https://doi.org/10.1039/C4CS00126E.

[83] J. Wang, Q. Zhang, F. Deng, X. Luo, D.D. Dionysiou, Rapid toxicity elimination of organic pollutants by the photocatalysis of environment-friendly and magnetically recoverable step-scheme SnFe2O4/ZnFe2O4 nano-heterojunctions, Chem. Eng. J. 379 (2020), 122264, https://doi.org/10.1016/j.cej.2019.122264.

[84] H.L. Tan, R. Amal, Y.H. Ng, Alternative strategies in improving the photocatalytic and photoelectrochemical activities of visible light-driven BiVO 4 : a review, J. Mater. Chem. A. 5 (2017) 16498–16521, https://doi.org/10.1039/C7TA04441K.

[85] A. Kudo, K. Omori, H. Kato, A novel aqueous process for preparation of crystal form-controlled and highly crystalline BiVO4 powder from layered vanadates at room temperature and its photocatalytic and photophysical properties, J. Am. Chem. Soc. 121 (1999) 11459–11467, https://doi.org/10.1021/JA992541Y.

[86] Z. Zhao, Z. Li, Z. Zou, Electronic structure and optical properties of monoclinic clinobisvanite BiVO4, Phys. Chem. Chem. Phys. 13 (2011) 4746, https://doi.org/10.1039/c0cp01871f.

[87] A. Walsh, Y. Yan, M.N. Huda, M.M. Al-Jassim, S.H. Wei, Band edge electronic structure of BiVO 4: elucidating the role of the Bi s and V d orbitals, Chem. Mater. 21 (2009) 547–551, https://doi.org/10.1021/CM802894Z.

[88] S. Stoughton, M. Showak, Q. Mao, P. Koirala, D.A. Hillsberry, S. Sallis, L. F. Kourkoutis, K. Nguyen, L.F.J. Piper, D.A. Tenne, N.J. Podraza, D.A. Muller, C. Adamo, D.G. Schlom, Adsorption-controlled growth of BiVO4 by molecular-beam epitaxy, APL Mater. (2013) 1, https://doi.org/10.1063/1.4824041.

[89] J.K. Cooper, S. Gul, F.M. Toma, L. Chen, P.A. Glans, J. Guo, J.W. Ager, J. Yano, I. D. Sharp, Electronic structure of monoclinic BiVO4, Chem. Mater. 26 (2014) 5365–5373, https://doi.org/10.1021/cm5025074.

[90] J.K. Cooper, S. Gul, F.M. Toma, L. Chen, Y.S. Liu, J. Guo, J.W. Ager, J. Yano, I. D. Sharp, Indirect bandgap and optical properties of monoclinic bismuth vanadate, J. Phys. Chem. C. 119 (2015) 2969–2974, https://doi.org/10.1021/jp512169w.

[91] S. Wang, X. Wang, B. Liu, Z. Guo, K. Ostrikov, L. Wang, W. Huang, Vacancy defect engineering of BiVO4 photoanodes for photoelectrochemical water splitting, Pubs. Rsc.Org 13 (2021) 17989, https://doi.org/10.1039/d1nr05691c.
[92] Y. Liu, B. Huang, Y. Dai, X. Zhang, X. Qin, M. Jiang, M.-H. Whangbo, Selective ethanol formation from photocatalytic reduction of carbon dioxide in water with BiVO4 photocatalyst, Catal. Commun. 11 (2009) 210–213, https://doi.org/10.1016/j.catcom.2009.10.010.
[93] Y. Park, K.J. McDonald, K.-S. Choi, Progress in bismuth vanadate photoanodes for use in solar water oxidation, Chem. Soc. Rev. 42 (2013) 2321–2337, https://doi.org/10.1039/C2CS35260E.
[94] X. Deng, R. Li, S. Wu, L. Wang, J. Hu, J. Ma, W. Jiang, N. Zhang, X. Zheng, C. Gao, L. Wang, Q. Zhang, J. Zhu, Y. Xiong, Metal–organic framework coating enhances the performance of Cu 2 O in photoelectrochemical CO2 reduction, J. Am. Chem. Soc. 141 (2019) 10924–10929, https://doi.org/10.1021/jacs.9b06239.
[95] H. Shen, M. Wang, X. Zhang, D. Li, G. Liu, W. Shi, 2D/2D/3D architecture Zscheme system for simultaneous H2 generation and antibiotic degradation, Fuel 280 (2020), 118618, https://doi.org/10.1016/j.fuel.2020.118618.
[96] J.C. Wang, L. Zhang, W.X. Fang, J. Ren, Y.Y. Li, H.C. Yao, J.S. Wang, Z.J. Li, Enhanced photoreduction CO2 activity over direct Z-Scheme α-Fe2O3/Cu2O heterostructures under visible light irradiation, ACS Appl. Mater. Interfaces. 7 (2015) 8631–8639, https://doi.org/10.1021/acsami.5b00822.
[97] C. Kim, K.M. Cho, A. Al-Saggaf, I. Gereige, H.T. Jung, Z-scheme photocatalytic CO2 conversion on three-dimensional BiVO4/carbon-coated Cu2O nanowire arrays under visible light, ACS Catal 8 (2018) 4170–4177, https://doi.org/10.1021/acscatal.8b00003.
[98] C. Zhou, S. Wang, Z. Zhao, Z. Shi, S. Yan, Z. Zou, A facet-dependent Schottky-Junction electron shuttle in a BiVO 4 {010}-Au-Cu 2 O Z-scheme photocatalyst for efficient charge separation, Adv. Funct. Mater. 28 (2018), 1801214, https://doi.org/10.1002/adfm.201801214.
[99] X. Li, D. Wei, L. Ye, Z. Li, Fabrication of Cu 2 O-RGO/BiVO 4 nanocomposite for simultaneous photocatalytic CO 2 reduction and benzyl alcohol oxidation under visible light, Inorg. Chem. Commun. 104 (2019) 171–177, https://doi.org/10.1016/j.inoche.2019.04.012.
[100] Z. Duan, X. Zhao, L. Chen, BiVO4/Cu0.4V2O5composites as a novel Z-scheme photocatalyst for visible-light-driven CO2conversion, J. Environ. Chem. Eng. 9 (2021), 104628, https://doi.org/10.1016/j.jece.2020.104628.
[101] S.K. Kuk, J. Jang, J. Kim, Y. Lee, Y.S. Kim, B. Koo, Y.W. Lee, J.W. Ko, B. Shin, J. K. Lee, C.B. Park, CO2-reductive, copper oxide-based photobiocathode for Z-scheme semi-artificial leaf structure, ChemSusChem. 13 (2020) 2940–2944, https://doi.org/10.1002/cssc.202000459.
[102] J. Li, W. Shao, M. Geng, S. Wan, M. Ou, Y. Chen, Combined Schottky junction and doping effect in CdxZn1-xS@Au/BiVO4 Z-Scheme photocatalyst with boosted carriers charge separation for CO2 reduction by H2O, J. Colloid Interface Sci. 606 (2022) 1469–1476, https://doi.org/10.1016/j.jcis.2021.08.103.
[103] X. Yu, F. Wen, F. Zhang, P. Yang, Y. Zhao, Y. Wu, Y. Wang, Z. Liu, Photocatalytic reduction of CO2 to CO over quinacridone/BiVO4 nanocomposites, ChemSusChem. 13 (2020) 5565–5570, https://doi.org/10.1002/cssc.202001764.
[104] J. Bian, Z. Zhang, J. Feng, M. Thangamuthu, F. Yang, L. Sun, Z. Li, Y. Qu, D. Tang, Z. Lin, F. Bai, J. Tang, L. Jing, Energy platform for directed charge transfer in the cascade Z-scheme heterojunction: CO 2 photoreduction without a cocatalyst, Angew. Chemie Int. Ed. 60 (2021) 20906–20914, https://doi.org/10.1002/anie.202106929.
[105] M. Lu, Q. Li, C. Zhang, X. Fan, L. Li, Y. Dong, G. Chen, H. Shi, Remarkable photocatalytic activity enhancement of CO2 conversion over 2D/2D g-C3N4/BiVO4 Z-scheme heterojunction promoted by efficient interfacial charge transfer, Carbon N. Y. 160 (2020) 342–352, https://doi.org/10.1016/j.carbon.2020.01.038.
[106] Q. Xie, W. He, S. Liu, C. Li, J. Zhang, P.K. Wong, Bifunctional S-scheme g-C3N4/Bi/BiVO4 hybrid photocatalysts toward artificial carbon cycling, Chinese J. Catal. 41 (2020) 140–153, https://doi.org/10.1016/S1872-2067(19)63481-9.
[107] A. Iwase, S. Yoshino, T. Takayama, Y.H. Ng, R. Amal, A. Kudo, Water splitting and co 2 reduction under visible light irradiation using z-scheme systems consisting of metal sulfides, coox-loaded bivo 4, and a reduced graphene oxide electron mediator, J. Am. Chem. Soc. 138 (2016) 10260–10264, https://doi.org/10.1021/jacs.6b05304.
[108] S. Yoshino, K. Sato, Y. Yamaguchi, A. Iwase, A. Kudo, Z-schematic co 2 reduction to co through interparticle electron transfer between srtio 3 :rh of a reducing photocatalyst and bivo 4 of a water oxidation photocatalyst under visible light, ACS Appl. Energy Mater. 3 (2020) 10001–10007, https://doi.org/10.1021/acsaem.0c01684.
[109] J. Bian, J. Feng, Z. Zhang, Z. Li, Y. Zhang, Y. Liu, S. Ali, Y. Qu, L. Bai, J. Xie, D. Tang, X. Li, F. Bai, J. Tang, L. Jing, Dimension-matched zinc phthalocyanine/BiVO 4 ultrathin nanocomposites for co 2 reduction as efficient wide-visible-light-driven photocatalysts via a cascade charge transfer, Angew. Chemie Int. Ed. 58 (2019) 10873–10878, https://doi.org/10.1002/anie.201905274.
[110] J. Bian, L. Sun, Z. Zhang, Z. Li, M. Chu, X. Li, D. Tang, L. Jing, Au-modulated z-scheme CuPc/BiVO 4 nanosheet heterojunctions toward efficient co 2 conversion under wide-visible-light irradiation, ACS Sustain. Chem. Eng. 9 (2021) 2400–2408, https://doi.org/10.1021/acssuschemeng.0c09256.
[111] Q. Han, L. Li, W. Gao, Y. Shen, L. Wang, Y. Zhang, X. Wang, Q. Shen, Y. Xiong, Y. Zhou, Z. Zou, Elegant construction of Znin2s4/bivo4hierarchical heterostructures as direct z-scheme photocatalysts for efficient co2photoreduction, ACS Appl. Mater. Interfaces. 13 (2021) 15092–15100, https://doi.org/10.1021/acsami.0c21266.
[112] J. Wu, L. Xiong, Y. Hu, Y. Yang, X. Zhang, T. Wang, Z. Tang, A. Sun, Y. Zhou, J. Shen, Z. Zou, Organic half-metal derived erythroid-like BiVO4/hm-C4N3 Z-Scheme photocatalyst: Reduction sites upgrading and rate-determining step modulation for overall CO2 and H2O conversion, Appl. Catal. B Environ. 295 (2021), 120277, https://doi.org/10.1016/j.apcatb.2021.120277.
[113] F. Kuttassery, H. Kumagai, R. Kamata, Y. Ebato, M. Higashi, H. Suzuki, R. Abe, O. Ishitani, Supramolecular photocatalysts fixed on the inside of the polypyrrole layer in dye sensitized molecular photocathodes: application to photocatalytic CO 2 reduction coupled with water oxidation, Chem. Sci. 12 (2021) 13216–13232, https://doi.org/10.1039/d1sc03756k.